



HAL
open science

Dating inset terraces and offset fans along the Dehshir Fault (Iran) combining cosmogenic and OSL methods

Kristell Le Dortz, Bertrand Meyer, Michel Sébrier, Regis Braucher, H. Nazari, L Benedetti, M. Fattahi, B. Bourlès, M. Foroutan, Lionel Siame, et al.

► To cite this version:

Kristell Le Dortz, Bertrand Meyer, Michel Sébrier, Regis Braucher, H. Nazari, et al.. Dating inset terraces and offset fans along the Dehshir Fault (Iran) combining cosmogenic and OSL methods. *Geophysical Journal International*, 2011, 185 (2), pp.1-28. 10.1111/j.1365-246X.2011.05010.x . hal-00590894

HAL Id: hal-00590894

<https://hal.science/hal-00590894>

Submitted on 16 May 2013

HAL is a multi-disciplinary open access archive for the deposit and dissemination of scientific research documents, whether they are published or not. The documents may come from teaching and research institutions in France or abroad, or from public or private research centers.

L'archive ouverte pluridisciplinaire **HAL**, est destinée au dépôt et à la diffusion de documents scientifiques de niveau recherche, publiés ou non, émanant des établissements d'enseignement et de recherche français ou étrangers, des laboratoires publics ou privés.

Dating inset terraces and offset fans along the Dehshir fault combining cosmogenic and OSL methods

K. Le Dortz^{1,2}, B. Meyer^{1,2}, M. Sébrier^{1,2}, R. Braucher³, H. Nazari⁴, L. Benedetti³, M. Fattahi^{5,6}, D. Bourlès³, M. Foroutan⁴, L. Siame³, A. Rashidi⁷, and M. D. Bateman⁶

1 - UPMC Univ Paris 06, ISTEP, UMR 7193, F-75005, Paris, France

2 - CNRS, ISTEP, UMR 7193; F-75005, Paris, France

3 - CEREGE UMR6635, Aix-En-provence, France

4- Research Institute for Earth Sciences, Geological Survey of Iran, PO Box 13185-1494 Tehran, Iran

5 - Institut of Geophysics, University of Tehran, Iran.

6 - Sheffield Centre for International Drylands Research, University of Sheffield, Sheffield S10 2TN, UK

7 - Geological Survey of Iran, PO Box 7615736841 Kerman, Iran

Abstract

¹⁰Be and ³⁶Cl cosmic ray exposure (CRE) and optically stimulated luminescence (OSL) dating of offset terraces have been performed to constrain the long-term slip-rate of the Dehshir fault. Analysis of cosmogenic ¹⁰Be and ³⁶Cl in 73 surface cobbles and 27 near-surface amalgams collected from inset terraces demonstrates the occurrence of a low denudation rate of 1 m.Ma⁻¹ and of a significant and variable inheritance from exposure prior to the aggradation of these alluvial terraces. The significant concentrations of cosmogenic nuclides measured in the cobbles collected within the riverbeds correspond to 72 ± 20 ka of inheritance. The mean CRE age of the surface samples collected on the older terrace T3 is 469 ± 88 ka but the analysis of the distribution of ¹⁰Be concentration in the near-surface samples discard ages older than 412 ka. The mean CRE age of the surface samples collected on terrace T2 is 175 ± 62 ka but the ¹⁰Be depth profile discard ages older than 107 ka. For each terrace, there is a statistical outlier with a younger age of 49.9 ± 3.3 ka and 235.5 ± 35.4 ka on T2 and T3 respectively. The late sediments aggraded before the abandonment of T2 and inset levels, T1 b and T1a, yielded optically stimulated luminescence (OSL) ages of respectively 26.9 ± 1.3 ka, 21.9 ± 1.5 ka, and 10.0 ± 0.6 ka. For a given terrace, the OSL ages, where available, provide ages that are systematically younger than the CRE ages. These discrepancies between the CRE and OSL ages exemplify the variability of the inheritance and indicate the youngest cobble on a terrace, that minimizes the inheritance, is the most appropriate CRE age for approaching that of terrace abandonment. However, the upper bound

39 on the age of abandonment of a terrace that is young with respect to the amount of inheritance
40 is best estimated by the OSL dating of the terrace material. For such terraces, the CRE
41 measurements are complementary of OSL dating and can be used to unravel the complex
42 history of weathering and transport in the catchment of desert alluvial fans. This
43 comprehensive set of dating is combined with morphological offsets ranging from 12 ± 2 m to
44 380 ± 20 m to demonstrate the Dehshir fault slips at a rate in the range 0.9 mm.yr^{-1} - 1.5
45 mm.yr^{-1} . The variable inheritance exemplified here may have significant implications for
46 CRE dating in arid endorheic plateaus such as Tibet and Altiplano.

47

47 **1. Introduction**

48 The Dehshir fault is a 380 km-long, strike-slip fault cutting through the Central Iran
49 plateau, north of the Zagros. It is located between 29.5°N-54.6°E and 33°N-53.1°E and is part
50 of a series of N-striking dextral faults slicing Central and Eastern Iran (e.g. Berberian, 1981).
51 The total offset of the fault, denoted by the geological offsets of the Nain Baft suture and the
52 Urumieh Doktor magmatic arc, amounts to 65 ± 15 km (Inset Figure 1; Walker and Jackson,
53 2004; Meyer et al., 2006). The southern portion of the Dehshir fault that runs across a series
54 of Quaternary alluvial fans shows clear evidence of recent right-lateral motion (Figure 1).
55 Geomorphologic studies have been performed to estimate the slip-rate of the fault. Combining
56 cumulative offsets of gullies and terrace risers with their inferred Holocene age, Meyer et al
57 (2006) and Meyer and Le Dortz (2007) suggested the fault slips at 2 mm.yr^{-1} . This initial
58 estimate has been further investigated by dating of optically stimulated luminescence (OSL)
59 samples collected within colluviums thought to predate the incision of an abandoned fan.
60 Nazari et al (2009) derived a minimum slip-rate of $0.8\text{-}2.5 \text{ mm.yr}^{-1}$ by combining the offset of
61 two gullies incised within the fan with the weighted mean OSL age of the colluviums.
62 However, neither the offset-gullies nor the surface of the abandoned fan have been dated
63 directly. Nazari et al. (2009) collected primarily the OSL samples for paleoseismic purpose,
64 within the fault zone where fanglomerate layers have been disrupted and/or warped.

65 In order to date the surface of the fan and provide further constraints on the slip-rate, we
66 have sampled the surface to estimate its cosmic ray exposure (CRE) age and the sediments
67 below the surface for OSL dating of their emplacement. While these two dating techniques
68 are commonly used separately, a few recent studies have combined luminescence dating with
69 cosmogenic data. In some cases the two methods yielded comparable ages though the CRE
70 ages are always slightly older than the OSL ones (e.g. Owen et al., 2003, 2006; De Long and
71 Arnold, 2007). Other studies yielded to significant differences, CRE ages being as much as
72 twice older than the OSL ones (Hetzl et al., 2004; Nissen et al., 2009; Le Dortz et al., 2009).
73 Some authors favoured the CRE ages whether they used surface samples only (Hetzl et al.,
74 2004) or near-surface samples only (Nissen et al., 2009). Others (Le Dortz et al., 2009) that
75 used both surface and near-surface samples concluded to a variable inheritance for the CRE
76 ages and favoured the OSL ages for dating the abandonment of alluvial surfaces.

77 We performed the sampling at two sites on the southern portion of the fault where
78 Meyer et al. (2006) documented right-lateral offsets of imbricate fan surfaces and riser cuts
79 (Figure 1). To constrain the age of the abandoned fan surfaces and the age of the subsequent

80 incision, we collected 100 samples (73 surface samples and 27 near-surface samples along
81 three profiles) to determine their CRE age by measuring the accumulation of ^{10}Be and ^{36}Cl
82 cosmogenic nuclides. Using two isotopes with markedly different half-lives offered the
83 opportunity to better constrain the erosion rate and evaluate the trade-off between erosion and
84 CRE age of the studied surfaces. We also collected six additional samples within quartz-rich
85 sandy layers located below alluvial surfaces to measure by OSL the time elapsed since the last
86 sunlight exposure of the sediment.

87 First, we describe the detailed morphology of the two sites with emphasis on inset
88 terrace levels imbricate within successive alluvial fan systems. Then, we present the results of
89 the CRE and OSL dating and discuss how far they help constraining the abandonment age of
90 the terrace treads and the age of the riser cuts that bound the treads. Finally, we discuss the
91 slip-rate of the Dehshir fault and the morphoclimatic chronology of the area.

92

93 **2. Offset Quaternary fans along the southern portion of the Dehshir fault**

94 **2.1 Site Dehshir South: Marvast River**

95 The Marvast River is the largest and the most active of the intermittent rivers draining
96 the study area, a dryland part of endorheic Central Iran Plateau. The river course is about 70
97 km long from its source within the High Zagros to the South of the Marvast city. The incision
98 of the Marvast River is limited because it vanishes into the Marvast salt flat, whose base level
99 stands at the elevation of 1520m. The drainage basin of the Marvast River is about 1100 km²,
100 and the upstream catchment drains several distinctive rock units including cover (Zagros
101 platform lithologies) and basement (Sanandaj Sirjan metamorphics). The river and its former
102 tributaries have emplaced the vast Quaternary piedmont made of coalescent fans that cover
103 most of the surface on the satellite imagery of figure 1. The recent incision of the piedmont
104 has resulted in a narrow channel supplying water to the city of Marvast, the formation of inset
105 terraces, and the fan head entrenchment. The Dehshir fault cuts across the Marvast River, the
106 active fans and the abandoned fan systems (Figure 2). To the west of Marvast city, several
107 inset terraces are distinguished (T0, T1a, T1b, T2, T3) and their relative age can be assessed
108 by their relative elevation (Figure 3). The material of each terrace, well layered, is of fluvial-
109 torrential origin and contains polygenic cobbles (Figure 3). The lower terrace T0 corresponds
110 to the present-day overflowing flood channel of the Marvast River. Many braided channels up
111 to 0.5-0.8 m deep incise T0. Very loose conglomerates alternate with silty-sandy layers. The
112 pebbles and the cobbles, either in the riverbed or on the surface of T0 are well rounded and
113 have not experienced cryoclasty. T1 is a terrace located 1 to 3 m above T0. T1 is made of two

114 distinctive levels, T1b slightly older and 1 m above T1a. Both T1a and T1b levels have been
115 probably emplaced during the same climatic period. They contain pebbles and well-rounded
116 cobbles with diameters up to 30 cm. The material is poorly cemented and some sandy layers
117 are found intercalated within the slightly indurate conglomeratic layers. Cobbles on the T1
118 surface display bar and swell morphology, most of them are well rounded very few have been
119 fragmented suggesting a very limited cryoclasty. T2 is an older terrace standing about 4-5 m
120 above T1 upstream of the Dehshir fault and 2-4 m above the present streambed downstream.
121 Several indurate sandy layers alternate with coarse conglomerates. T2 surface is flat and many
122 fragmented cobbles are found on it, suggesting that the terrace underwent low temperatures
123 and contrasted seasons during long period of times associated with strong wind deflation, as
124 under glacial climates. The upper part of the terrace is fairly cemented by a discontinuous
125 calcrete up to 1 m thick at some places. T3 is the top surface of the highest alluvial fan
126 system. It stands more than 5 m above T2. Where exposed upstream, by the Marvast incision,
127 T3 contains many cryoclasted cobbles and a few large cobbles. The conglomerate levels are
128 strongly indurate and the upper part of T3 is cemented by a continuous, 0.4-0.8 m thick,
129 reddish calcrete. Numerous gelifracted cobbles can be found on its surface. Many gullies
130 incise T3; they are deeper and wider than the shallow immature rills incising T2. The overall
131 terrace has a characteristic striped-morphology on the satellite imagery with flat strips
132 separated by narrow intervening intermittent gullies (Figure 2).

133 There are also a few remnants of older conglomerates cropping out close to the fault
134 (Figure 2). These older conglomerates are assigned to the Pliocene according to the geological
135 mapping by GSI (1981). The layers are mostly tilted to the west and squeezed within the fault
136 zone, but the orientation of the cobbles indicates an eastward paleocurrent direction (Meyer et
137 al., 2006). The successive fans have been all emplaced by the Marvast River and
138 progressively deformed through time. The most recent riser cut of the Marvast river stands
139 between T1 tread and the river course (T1b/T0) West of the fault and between T2 tread and
140 the river course (T2/T0) East of the fault. This T2/T0 riser, deflected in a right-lateral sense
141 by an amount of 25 ± 5 m, is not a passive marker and might have been rejuvenated by lateral
142 erosion (Figure 2a). Several larger offsets occur further to the South. About 2 km south of the
143 Marvast River, a large dry river, deeply incised within the oldest fan T3, is right-laterally
144 offset by 380 ± 20 m (Figure 2b). This offset is higher than the 180-200m offset streams
145 described by Meyer et al. (2006) a little further to the South. The latter offsets correspond to
146 streams that are narrower and less incised than for the former. Consequently, the value of 380

147 ± 20 m corresponds to the largest dextral offset observed amongst the many rivers incising T3
148 and provides a minimum bound of the fault motion since the abandonment of T3 tread.

149

150

2.2 Site Dehshir North

151 The site Dehshir North is located about 25 km north of the Marvast River (Figure 1).
152 The site lies close to a 30 km long, north-south trending, intermittent stream in which present-
153 day drainage is mostly restricted to the northern part of the piedmont. The stream is
154 disconnected from the Marvast River but it grades almost back to the Marvast River outlet
155 from the Sanandaj Sirjan Mountains and drains a significant area of the Quaternary piedmont.
156 At site Dehshir North, the piedmont mainly consists of the distal part of the abandoned fan T3
157 (Figure 4). Similarly to the site Dehshir South, several lower levels (T2, T1b, T1a) with
158 limited extension are nested within the alluvial fan T3. The material of each terrace is also of
159 fluvial-torrential origin but the gravel sizes are smaller than at site Dehshir South. Fine
160 content is higher and the coarser levels are void of boulders.

161 The higher level T3, although much resembling that along the Marvast River on the
162 SPOT Imagery, has been a little less incised and dissected by the rivers than at Dehshir South.
163 At Dehshir North, T3 stands about 4 m only above the active riverbed (Figure 4b) and its
164 surface displays many cryoclasted cobbles. T3 is incised upstream by many short gullies
165 regularly spaced every 20-30 m. Such gullies probably formed as a result of regressive
166 erosion after the abandonment of the terrace T3 and the cutting of the risers. T2 has a very
167 limited extension with respect to T3. It is a lateral fan sloping down gently northward that was
168 aggraded by small local tributaries that are incised within T3 terrace and rework its alluvial
169 material. T2 surface stands 2-4 m below T3 and is much less incised than the old terrace; only
170 a few short gullies irregularly spaced are distinguished on the Quickbird Imagery (Figure 4a).
171 As T3, the surface of T2 displays cryoclastic material. The emplacement of the lateral fan T2
172 is partly controlled by the local development of the Dehshir fault. The terrace T1 lies 1 m at
173 most below the terrace T2 and stands 1 m above the riverbed T0. Most of the gullies that
174 incise T3 and T2 merge downstream with T1 and their incision is probably synchronous with
175 the emplacement of T1. The surface of T1 displays only very few cryoclasted cobbles.
176 Similarly to the site Dehshir South, two levels (T1a and T1b) can be distinguished, with T1b
177 being older and standing 0.5-1 m above T1a. Both the terrace T1 and the lateral fan T2 are
178 nested in the highest terrace T3 and have a very limited extent.

179 Some small gullies that incise T3 and T2 cross the fault zone at a right angle. Two of
180 these gullies are clearly offset in a right-lateral sense by 20-30 m (figure 4), an amount similar

181 to the deflection of the Marvast River at the site Dehshir South. These gullies postdate the
182 emplacement of T3 and T2 and might have formed as a result of regressive erosion since the
183 last significant incision of the network. Their incision is probably coeval with the
184 emplacement of the terrace T1 with which they merge downstream, and the gullies, according
185 to weighted mean OSL dating in a trench within the fault zone, are supposed to be younger
186 than 21.1 ± 11.2 ka (Nazari et al., 2009). There is also an offset of the right bank of the main
187 river flood channel (Figure 5). Upstream, the most recent riser cut (T3/T0) stands between T3
188 tread and the riverbed. Downstream, T1 is protected from erosion because of the right-lateral
189 motion of the fault and the most recent riser stands between T1 tread and the riverbed
190 (T1a/T0). The riser that postdates the terrace T1a is offset by 12 ± 2 m (Figure 5).

191

192

3. Chronology of the regional fans

193 The dating of the alluvial surfaces and inset terraces at both sites is required to establish
194 the chronology of the fans and constrain the age of the offset-risers. Two complementary
195 dating methods, cosmic ray exposure (CRE) and optically stimulated luminescence (OSL),
196 have been performed to estimate the age of abandonment of alluvial surfaces. OSL relies on
197 natural background radioactivity of the material with a small contribution of cosmogenic
198 radiation and measures the time elapsed since the last sunlight exposure of a sediment layer.
199 CRE provides the time of exposure of superficial material to cosmic rays.

200

3.1 Sampling strategy and analytical procedures for cosmogenic and OSL dating

201 All the terraces (T0, T1, T2 and T3) were sampled at each site for cosmogenic dating.
202 For some surfaces (T3 at sites Dehshir North and Dehshir South, T2 at site Dehshir South)
203 and taking advantage of the occurrence of polygenic cobbles, both the ^{10}Be and ^{36}Cl
204 cosmogenic nuclides dating techniques have been applied. We measured the concentrations of
205 *in-situ* produced ^{10}Be and ^{36}Cl accumulated respectively in quartz-rich and carbonates samples
206 exposed to cosmic rays. Surface samples were collected to estimate the CRE ages (Table 1).
207 Most of the surface samples, 67 over the 73 collected, consists of individual cobbles, 4
208 correspond to two fragments of the same gelifracted cobble, and 2 only are amalgams of
209 many (about 25) pieces of small pebbles. Near-surface samples were also collected along
210 three profiles to estimate the inheritance, i.e., the concentrations of cosmogenic nuclides
211 accumulated in the cobbles prior to their deposition. Each near-surface sample is an amalgam
212 of pebbles or fragments of cobbles collected at the same depth. Provided that the sediment
213 emplaced in a short period of time and that the pre-exposure is homogeneous, the exponential
214

215 decrease of concentrations with depth provides an estimate of the homogeneous inheritance
216 (e.g. Anderson et al., 1996; Repka et al., 1997). The inherited concentration is determined
217 from the asymptotic value that the profile tends to at depth and a chi-square inversion is often
218 used to minimise the differences between measured and modelled concentrations (e.g., Siame
219 et al., 2004; Braucher et al., 2009). Collecting pebbles from the active streambed also helps to
220 estimate the inherited component (e.g. Brown et al., 1998). However, this method relies on
221 the questionable assumption that the pre-depositional history of the pebbles collected in the
222 present-day streambed is comparable to that of the pebbles collected on abandoned fan
223 surfaces during aggradation stages.

224

225 Three main types of secondary particles are involved in the *in situ* production of ^{10}Be :
226 fast nucleons (essentially neutrons), stopping (or negative) muons and fast muons. Each of
227 them has its own effective attenuation length. We used in this paper the same parameters as
228 Braucher *et al.* (2003) for the muonic attenuation lengths that are 1500 g.cm^{-2} for stopping
229 muons and 5300 g.cm^{-2} for fast muons. For fast neutron, an attenuation length of 160 g.cm^{-2}
230 (Gosse and Phillips, 2001) is used rather than the attenuation length of 177 g.cm^{-2} (Farber et
231 al., 2008) modelled at mid-latitude in California but without accounting for the muonic
232 contribution. Samples were prepared at the CEREGE laboratory in Aix-en-Provence for ^{10}Be
233 concentration measurements following chemical procedures adapted from Brown et al. (1991)
234 and Merchel and Herpers (1999). After addition in each sample of $\sim 100 \mu\text{l}$ of an in-house
235 $3.10^{-3} \text{ g/g } ^9\text{Be}$ carrier solution prepared from deep-mined phenakite (Merchel et al., 2008), all
236 ^{10}Be concentrations were normalized to $^{10}\text{Be}/^9\text{Be}$ SRM 4325 NIST standard with an assigned
237 value of $(2.79 \pm 0.03).10^{-11}$. This standardization is equivalent to 07KNSTD within rounding
238 error. All ^{10}Be data reported in this study (Table 1) have been measured at ASTER
239 (CEREGE, Aix-en-Provence). Analytical uncertainties (reported as 1σ) include uncertainties
240 associated with AMS counting statistics, AMS external error (0.5%), chemical blank
241 measurement. Long term measurements of chemically processed blank yield ratios on the
242 order of $(3.0 \pm 1.5).10^{-15}$ (Arnold et al., 2010). Cosmocalc add-in for excel (Vermeesch, 2007)
243 has been used to calculate sample scaling and standard atmospheric pressures. Stone (2000)
244 polynomial has been used to determine surficial production rate assuming a SLHL production
245 rate of $4.49 \text{ at.g}^{-1}.\text{yr}^{-1}$ for ^{10}Be .

246

247 ^{36}Cl can be produced by two mechanisms in superficial rocks, cosmic ray interactions
248 (spallation reactions of Ca, K, Ti and Fe, capture of low energy epithermal and thermal
249 neutrons by ^{35}Cl , and direct capture of slow negative muons by K and Ca) and radiogenic
250 production by disintegration of U and Th. To determine the proportion of radiogenic ^{36}Cl
251 requires measuring the concentrations of U and Th in the target mineral (Zreda et al., 1991;
252 Stone et al., 1996, 1998; Gosse & Phillips 2001; Schimmelpfennig et al., 2009). Major
253 elemental compositions of rock samples were determined by ICP-OES technique by the
254 CNRS service for rocks and minerals analysis at CRPG Nancy. For the ^{36}Cl measurements,
255 the chemical extraction of chlorine by precipitation of silver chloride has been adapted from
256 the protocol of Stone et al. (1996). The samples were spiked with a known quantity of stable
257 chlorine carrier (e.g. Desilets et al., 2006) to simultaneously determine ^{36}Cl and chlorine
258 concentrations by isotope dilution accelerator mass spectrometry (AMS). The chemical
259 treatment of the samples was carried out at the CEREGE laboratory in Aix-en-Provence and
260 the measurements were performed at the Lawrence Livermore National Laboratory, using
261 KNSTD1600 standard. The excel spreadsheet provided by Schimmelpfennig et al., (2009)
262 was used to calculate all ^{36}Cl production rates and to model ^{36}Cl data. Accordingly, a surface
263 spallation rate of $48.8 \pm 3.4 \text{ at.g}^{-1}(\text{Ca}).\text{yr}^{-1}$ (Stone et al. 1996) is used. However we use a
264 neutron attenuation length of 160 g.cm^{-2} (Gosse & Phillips 2001) instead of 177 g.cm^{-2}
265 (Farber et al., 2008) as explained above and for self consistency. The concentrations of *in-situ*
266 produced ^{10}Be and ^{36}Cl are given in Table 1 and the chemical composition of the carbonate
267 samples in Table 2.

268

269 Optically stimulated luminescence was used to date the alluvial layers emplaced during
270 the aggradation of the fans. Lenses of fine sandy-silts intercalated between conglomerates at
271 various depths below the surface were sampled for OSL in opaque tubes. The Single Aliquot
272 Regeneration (SAR) protocol (e.g.; Murray and Wintle, 2000) was employed for the
273 Equivalent dose (De) measurement once quartz had been extracted and cleaned from each
274 sample. The analytical procedures employed are identical to that applied to similar samples
275 from the neighbouring Anar, Sabzevar and Doruneh areas (Le Dortz et al., 2009; Fattahi et al,
276 2006; 2007).

277 Initial attempts to use single grains for De determination failed due to the dimness of
278 OSL signal. As a result De measurements were undertaken on 9.6 mm diameter aliquots
279 containing approximately 1500-2000 grains. Whilst normally this might result in averaging

280 out of any multiple dose component within a sample, here it is assumed that for these dim
281 samples the luminescence signal from each aliquot was produced by a relatively few number
282 of bright grains and thus may be considered as almost measuring at single grain level.
283 Therefore, the De distribution of the single aliquot De measurements is considered to be
284 almost a true reflection of the actual De distribution within a sample. For some samples the
285 depositional setting, field sedimentary logs and the scatter of the replicate aliquot De data
286 indicated that prior to burial, full resetting (bleaching) of the OSL signal had not taken place
287 and/or that the sediments had undergone some post-depositional disturbance (Bateman et al.,
288 2007). As a result of this, Finite Mixture Model (FMM; Roberts et al. 2000) was used where
289 samples showed skewed, scattered, or multimodal distributions. We used the dominant FMM
290 component for samples displaying multimodal De distributions and the lowest FMM
291 component of De for samples whose De distributions were skewed (assuming partially
292 bleached without significant bioturbation) samples (Boulter et al., 2007; Bateman et al.,
293 2007). Where samples had a low over-dispersion and unimodal, normally distributed De's
294 then the Central Age Model (CAM; Galbraith et al., 1999) De was used for age calculation
295 purposes. The relevant information for OSL ages are presented in Table 3 in years from
296 present with 1 sigma errors.

297
298
299

300 **3.2 Cosmic ray exposure ages**

301 Figure 6 displays the results for the site Dehshir North, and figure 7 for the site Dehshir
302 South. The concentrations are given in Table 1 with the corresponding CRE ages modelled
303 assuming erosion and inheritance are negligible.

304

305

3.2.1 Surface T3

306 For T3, both the ^{10}Be and ^{36}Cl zero-erosion, zero-inheritance ages of surface samples are
307 overall consistent and suggest that the terrace tread is old.

308 At Dehshir North (Figure 6), the CRE ages range between 235 and 519 ka for the ^{10}Be
309 measurements, and between 268 and 383 ka for the ^{36}Cl measurements. For the ^{10}Be
310 concentrations, all but one surface sample provide CRE ages greater than 400 ka. The younger
311 ^{10}Be exposure age (DN06S2, 235.5 ± 35.4 ka) might be considered as an outlier and excluded
312 from the statistics. Then, the weighted mean of the zero-erosion zero-inheritance ^{10}Be model
313 age of T3 is 462 ± 55 ka while the ^{36}Cl one is 325 ± 74 ka (Figure 6b).

314 At site Dehshir South (Figure 7), the scattering of the concentrations is greater. The
315 weighted means of the zero-erosion zero-inheritance ^{10}Be and ^{36}Cl ages are 481 ± 119 and 344
316 ± 83 ka, respectively (Figure 7b). The results are nonetheless similar at both sites and confirm
317 the qualitative inference of the synchronism of levels T3 drawn from the resemblance of their
318 surface at distant sites on the Quickbird imagery. They indicate T3 is a rather old surface
319 (several hundreds ka) and that ^{36}Cl surface ages are a little younger than ^{10}Be ages. The slight
320 difference between the ^{10}Be and ^{36}Cl weighted mean ages may either result from a statistical
321 bias due to the limited number of samples or be meaningful. The ^{36}Cl half-life (301 ka, e.g.
322 Gosse & Philipps, 2001) being lower than that of ^{10}Be (1.387 ± 0.12 Ma, Chmeleff et al.,
323 2009; Korshinek et al., 2009) and T3 an old terrace, the difference may suggest the carbonates
324 have reached the steady-state equilibrium for which the production of ^{36}Cl is balanced by the
325 loss due to radioactive decay and the loss due to erosion, if there is any.

326 Because there is a trade-off between denudation rate and exposure age, it is important to
327 estimate the erosion. Assuming an infinite age for the emplacement of T3 allows estimating a
328 maximum erosion rate for each of the surface samples, both for ^{36}Cl and ^{10}Be isotopes (Table
329 1). For the carbonates, none of the surface samples provides a ^{36}Cl maximum denudation rate
330 greater than 2.1 m.Ma^{-1} , and the averaged value is 1.5 m.Ma^{-1} . Discarding the outlier DN06S2,
331 the quartz surface samples indicate a ^{10}Be maximum denudation rate smaller than 1.6 m.Ma^{-1}
332 with an averaged value of 1.4 m.Ma^{-1} . This is further strengthened by modelling the depth-
333 distribution of the ^{36}Cl concentrations in the amalgamated carbonate samples collected along a
334 3 m depth profile excavated in T3 at the site Dehshir North (Figure 8). The profile shows an
335 overall exponential decrease of concentrations with depth allowing for modelling the erosion
336 rate. The ^{36}Cl concentration depth profile is modelled with assigning a surface age of 3 Ma;
337 old enough to ascertain the equilibrium between production and disintegration has been
338 reached. Letting the erosion rate and the inheritance free to vary, the profile is modelled for
339 three density values (between 2 and 2.4 g.cm^{-3}) within the range of that measured for the
340 samples of the profile (Figure 8). For all the densities tested, the model converges towards
341 zero inheritance solutions and low erosion rates. The solutions with zero inheritance are not
342 surprising because the assigned surface age of 3 Ma makes a homogeneous inheritance of
343 several tens of ka undetectable. By contrast, the solutions with low maximum erosion rates
344 are meaningful. The greatest erosion rate of 1.90 m.Ma^{-1} is obtained for a density value of 2
345 g.cm^{-3} . Smaller erosion rates of 1.48 and 1.18 m.Ma^{-1} corresponding to densities of 2.2 and 2.4

346 g.cm^{-3} are closer to the erosion rate calculated for each of the carbonate surface samples (Table
347 1).

348 Whatever the method applied (surface sample, near-surface samples and depth-profile
349 modelling) and whatever the isotope considered, the estimates of the maximum erosion rate
350 are very low. They are close to that found in hyperarid regions ($<1 \text{ m.Ma}^{-1}$, Matmon et al.,
351 2009) and in good agreement with the pristine morphology of the flat-topped surface of T3.
352 The ^{10}Be depth profile can be theoretically modelled with erosion rates ranging between 0 and
353 1.4 m.Ma^{-1} , maximum erosion rate averaged from the ^{10}Be surface samples. Accounting for
354 the trade-off between erosion rate and exposure age (the higher the erosion rate, the older the
355 exposure age), the ^{10}Be depth profile has been modelled under the assumption of no erosion to
356 minimize the exposure age. We hence tested a range of inheritance values to solve for the zero
357 erosion exposure age (Figure 9). The best fit is obtained for a surface age of 464 ka and a
358 homogeneous inheritance of $3.8 \cdot 10^5 \text{ at.g}^{-1}(\text{SiO}_2)$. This inheritance, if acquired at the surface
359 and prior to the emplacement of the terrace, would correspond to a period of pre exposure of
360 about 32 ka, small with respect to the exposure age. Accounting for the trade-off between
361 inheritance and age, several other solutions remain acceptable (Figure 9b). Assuming a
362 homogeneous inherited concentration of $7.6 \cdot 10^5 \text{ at.g}^{-1}(\text{SiO}_2)$, twice that obtained for the best
363 fit and close to the concentration measured for the deepest sample of the profile, provides an
364 age of 327 ka. Hypothesizing zero inheritance yields an older age of 686 ka that does not
365 match with the concentrations of surface samples, demonstrating the usefulness of combining
366 both surface and near-surface sampling.

367 In summary, T3 is a rather old and well-preserved alluvial surface, in which cobbles
368 have incorporated a poorly constrained inheritance of several tens of ka. This amount of
369 inheritance, though limited with respect to the CRE age of T3, contributes to the $469 \pm 88 \text{ ka}$
370 weighted mean age of all the quartz cobbles collected on the terrace tread at sites Dehshir
371 North and Dehshir South (Figure 10).

372

373

3.2.2 Surface T2

374 At Dehshir North, only one amalgam quartz-rich surface sample has been dated on T2
375 fan surface. The zero-erosion zero-inheritance CRE age is $406.5 \pm 26.5 \text{ ka}$ (Table 1, Figure
376 6a). This age is a little younger than of the weighted mean age of T3 and agrees with the
377 assumption that T2 aggradation at this site results from reworking of T3 material. Indeed, T2
378 CRE age is older than several ages that have been used to estimate the weighted mean age of
379 T3 and much older than that of the T3 outlier. At Dehshir South, twelve samples collected on

380 T2 have been analysed (Figure 2a and Figure 7). The ^{10}Be and ^{36}Cl concentrations, hence the
381 corresponding CRE ages calculated assuming zero-erosion and zero-inheritance are scattered
382 (Table 1, Figure 7a). The CRE ages of the surface samples range between 49.9 ± 3.3 and
383 225.8 ± 14.7 ka for the ^{10}Be and between 104.4 ± 10.5 and 190.3 ± 20.8 ka for the ^{36}Cl . The
384 youngest ^{10}Be CRE age on T2 (DS08S114, 49.9 ± 3.3 ka) might be considered as an outlier
385 and excluded from the statistics. Discarding the outlier and keeping in mind the limited
386 number of samples, the ages remain scattered without significant differences between ^{10}Be
387 and ^{36}Cl ages. The distribution is multimodal with a weighted mean CRE age of 175 ± 62 ka
388 (Figure 11a). This average is consistent with the intermediate elevation of T2 terrace and its
389 surface characteristics as well as the fact that none of the CRE ages obtained for T2 is older
390 than the youngest age calculated for T3.

391 Amalgamated samples have also been collected along two depth profiles at site
392 Dehshir South. The ^{10}Be concentrations are listed in Table 1. The profile PS1 was collected by
393 the riser between T2 and the Marvast riverbed, 300 meters East of the fault zone (Figures 2
394 and 11). The profile PS2 has been collected 1.5 kilometres NE of PS1, close to the fault scarp
395 in a pit dug within the T2 surface and nearby remnants of T3 (Figures 2 and 12). For both
396 profiles, the uneven distribution of the ^{10}Be concentrations dismisses a uniform pre-exposure
397 prior to the emplacement of T2 material and precludes any appropriate modelling of a
398 homogeneous inheritance. As for the study of alluvial surfaces in the Anar neighbouring area
399 (Le Dortz et al., 2009), the profile data, together with the scattering of the concentrations of
400 the surface cobbles, suggest the occurrence of a variable inheritance.

401

402

3.2.3 Surface T1 and T0

403 At site Dehshir North, the four surface samples collected on T1a provide CRE ages
404 ranging between 82 and 424 ka (Figures 4 and 6a). The sample with the oldest age might be
405 considered an outlier and the CRE age of the terrace would be better determined by the three
406 youngest samples and bracketed between 82 and 134 ka. The T1a outlier has an age close to
407 that of the amalgam on T2 fan surface and close to that of the surface samples collected on
408 T3. This suggests that the T1a outlier is a T2 or T3 cobble reworked by the small gullies
409 incising the surface of T2 and T3 treads and which incision is coeval with the emplacement of
410 T1.

411 At site Dehshir South, the four surface samples have been collected on T1b. They
412 provide ^{10}Be exposure ages ranging between 30 and 318 ka (Figures 2 and 7a). The oldest
413 sample, even older than the samples collected on T2 tread, is as an outlier. Either it is a

414 former cobble of T3 locally reworked by the small gullies incising T3 or a cobble exposed to
415 cosmic rays for a long time in the upstream catchment of the Marvast River. In any case, such
416 an outlier indicates that the inheritance of individual cobbles collected on T1 tread can be
417 very important. Of the three remaining samples collected on T1b, two provide CRE ages that
418 are not distinguishable from the CRE weighted mean age (175 ± 62 ka) of T2, the terrace
419 immediately above. Only one sample (DS08S124, 32.1 ± 2.1 ka) provides an age
420 significantly younger than the ages on T2. This CRE age on T1b surface is significantly
421 younger than the CRE ages on the T1a surface at site Dehshir North, suggesting that at this
422 latter location, the surface cobbles of the T1a terrace contain an important amount of inherited
423 ^{10}Be .

424 At site Dehshir South, five samples have been collected in the present day streambed of
425 the Marvast River. Whatever the isotope considered, all provide non-zero CRE ages ranging
426 between 54 and 96 ka, suggesting the occurrence of a significant inheritance. The CRE ages
427 of T0 are younger than the CRE ages of T1b except for the youngest sample of T1b
428 (DS08S124, 32.1 ± 2.1 ka). At site Dehshir North, four samples have been collected in the
429 main river flood plain T0. Discarding the outlier, three samples (two ^{10}Be ages and one ^{36}Cl
430 age) provide non-zero CRE ages ranging between 57 and 84 ka, confirming the occurrence of
431 a significant inheritance averaging some 70 ka. When including the outlier corresponding to
432 the oldest sample collected in the river, the scattering of the concentrations increases and
433 suggests the pre exposure history of a cobble before the abandonment of an alluvial surface is
434 highly variable.

435 To summarize (Figure 13a), the observed average inheritance in the present stream
436 beds of some 70 ka, as well as the distribution of CRE ages for the inset levels T1 and T2,
437 suggest that T1 and T2 treads are likely to be younger than their CRE weighted mean age.
438 Thus, the ages of abandonment of the terrace treads may be better approximated by the CRE
439 age of the youngest sample found on each surface. Such a conclusion has already been drawn
440 for alluvial fan surfaces in the neighbouring region of Anar (Le Dortz et al., 2009).

441

442 **3.3 Optically stimulated luminescence ages**

443 OSL dating was performed to better constrain the chronology of alluvial terraces at the
444 two studied sites. Five OSL samples initially sought to determine the ages of faulted deposits
445 for paleoseismology purposes were sampled at site Dehshir North (Nazari et al., 2009). Then,
446 six new OSL samples were collected at site Dehshir South. As no suitable material was found
447 within old terrace T3, OSL ages help only constraining the aggradation timing of terraces T2

448 and T1; they also permit comparison with CRE ages. The ages of all the OSL samples,
449 including those previously published by Nazari et al. (2009), have been recalculated in section
450 3.1 using CAM or FMM techniques to account for the scatter of the De distributions.

451 OSL samples were collected at site Dehshir North, in a trench excavated within T3
452 and T2 (Figure 4 in Nazari et al., 2009). Within this trench, the distal alluvial and colluvial
453 deposits corresponding to the T2 and subsequent levels provide refined OSL ages of $60.0 \pm$
454 5.7 ka, 45.5 ± 4.6 ka, and 20.1 ± 1.6 in accord with the stratigraphic succession (Table 3,
455 sample HI/2008-IX in unit E1, sample HI/2008-VII in unit D3b, sample HI/2008-VIII in unit
456 D4, Nazari et al., 2009). In addition, recent colluviums incised by small streams flowing
457 through the Dehshir fault zone and which base level matches with the tread of T1 yielded two
458 OSL ages of 26.0 ± 1.0 ka for the lower colluviums and 20.2 ± 0.8 for the upper ones (Table
459 3, sample HI/2008-I in unit B1 and sample HI/2008-VI in unit B2, Fattahi et al., 2010). These
460 two latter OSL ages, which postdate the incision of T2, are coeval with the emplacement of
461 T1. They imply that the T1b tread, all the more the T1a tread, is at most 21 ka (oldest possible
462 age of the most superficial sample). Notwithstanding that the OSL samples have not been
463 directly collected under the terrace treads sampled for CRE dating, the data available at site
464 Dehshir North indicate large discrepancies between the CRE and OSL ages. The cannibalism
465 of the old T3 terrace by subsequent alluvial deposits may explain such discrepancies by
466 locally recycling T3 cobbles during the aggradation of the lower terraces T2 and T1. This
467 possibility is further examined at site Dehshir South for which OSL samples have been taken
468 right below the terrace treads T2 and T1 where sampled for CRE dating.

469 For T2 at Dehshir South, two OSL samples, OSL I and OSL II, have been collected
470 from the riser between T2 and the active riverbed, very close to the profile PS1 (Figure 2a and
471 11b). OSL I has been collected 15 m to the West of PS1 and at a depth of 0.8 (OSL I) and
472 OSL II, 10 m to the East of PS1 and at a depth of 3.4 m. The samples OSL I and II yielded
473 ages of 26.9 ± 1.3 ka and 29.4 ± 5.1 ka, respectively (Table 3). These similar OSL ages
474 suggest that the material of the terrace T2 emplaced rapidly and that its tread is at most 28.2
475 ka. The OSL samples of the riser T2/T0 provide ages much younger than the weighted mean
476 ^{10}Be and ^{36}Cl CRE age of T2, 175 ± 62 ka (Figure 11a), but closer to 49.9 ± 3.3 ka, the
477 youngest CRE age on T2 tread (DS08S114 in Table 1). Two additional OSL samples
478 (AB/2006-I and II in Table 3) were collected within a colluvium pediment topping T2 in the
479 pit of profile PS2 (Figure 2a and 12b). These samples yielded OSL ages of 39.7 ± 2.6 and
480 20.0 ± 1.3 which confirm this desert pediment was formed both by the end of the
481 emplacement of terrace T2 and after its abandonment. To summarize, the OSL ages obtained

482 for T2 indicate its aggradation occurred during the time-interval 25.6-65.7 ka. This suggest
483 that the samples collected on T2 tread, providing exposure ages older than 66 ka, contain an
484 inherited CRE component, For T1, two OSL samples, OSL III and IV, were collected at
485 Dehshir South in fine sands respectively below the surface of T1b and T1a (Figure 3b). The
486 error bars on sample OSL III, taken by the riser T1b/T0, provide minimum and maximum
487 OSL ages of 20.4 ka and 23.4 ka for the T1b tread. The sample OSL IV, taken by the riser
488 T1a/T0, provides minimum and maximum OSL ages of 9.4 ka and 10.6 ka for the T1a tread.
489 These ages are in agreement with the relative elevation of the terraces, the samples from the
490 riser T2/T0 being older than the sample from the riser T1b/T0, itself older than the sample
491 from the riser T1a/T0. Similarly to the terrace T2, the OSL age of T1b is younger than the
492 ^{10}Be CRE ages of the samples collected on the T1b tread. This OSL age is almost one order of
493 magnitude younger than the three oldest ^{10}Be samples and 30% younger than the youngest
494 ^{10}Be sample (DS08S114). There is no direct comparison available between OSL and CRE
495 ages for T1a because this surface has not been sampled for cosmogenic dating.

496 At the two studied sites along the Dehshir fault, the OSL ages on terraces T2 and T1
497 are systematically younger than the CRE ones on the same terrace. For a given terrace, the
498 CRE statistical outlier, which is the youngest CRE age and has been consequently removed
499 from the calculation of the weighted mean CRE age, remains slightly older than, but closer to
500 the OSL ages. Two extreme options may be contemplated: either OSL ages have been
501 rejuvenated or CRE concentrations include a high percentage of inheritance. Most of the
502 physical processes that are known to affect the OSL method, such as partial bleaching,
503 incorporate an antecedent signal leading to overestimation of the age of sediment burial. This
504 has been accounted for the studied samples by the statistical processing of the De
505 distributions. Conversely, OSL signal is sensitive to the temperature and a loss of
506 luminescence might occur at temperatures above 50°- 60°C. Such temperatures may occur on
507 the Iran plateau during summertime so that OSL ages could be theoretically rejuvenated.
508 Nevertheless, to account for gamma rays shielding, OSL samples were taken at least at 0.7 m
509 below the ground surface (Table 3), a depth large enough to prevent strong variations of
510 temperature. In addition, if temperature had affected the OSL signal, such effect would
511 decrease with increasing sampling depth. However, no trade-off is observed between the OSL
512 ages and the sampling depth (Table 3). On the contrary, OSL ages, whatever the depth, appear
513 similar for the same terrace and in agreement with the relative elevation of the terraces. As a
514 consequence, the variable inheritance of CRE concentrations should chiefly explain the
515 discrepancy with OSL ages.

516

517

3.4 Discussion on the abandonment age of the alluvial surfaces

518

519

520

521

522

523

524

525

526

527

528

529

3.4.1 Variable CRE inheritance and maximum abandonment ages of alluvial treads.

530

531

532

533

534

535

536

537

538

539

540

541

542

543

544

545

546

547

548

549

The overall chronology of the fan surfaces crossed by the Dehshir fault has been established but the abandonment age of each surface is not easily assigned for several reasons (Figure 13). First, the scattering of CRE concentrations on a given surface, the occurrence of more concentrated samples on younger surfaces than on older ones, the occurrence of significant concentrations in active river beds, indicate there is a variable inheritance uneasy to account for. Second, where CRE and OSL data are available for the same terrace, the OSL ages of the late sediments of the terrace are always much younger than the CRE ages of the cobbles abandoned on its tread. Such disparities between OSL and CRE ages appear to result from the high variability of the CRE inheritance that needs further consideration.

A rough estimate of the variable inheritance is provided by the CRE weighted mean of 72 ± 20 ka obtained from 8 of the 9 samples collected in the riverbeds once the oldest outlier discarded. Moreover, amalgam sample DS08P130 from profile PS1 (Figure 11c) has a measured concentration (Table 1) of $8.86 \cdot 10^5$ at.g⁻¹(SiO₂), even though it is located at 2.1 m below the T2 surface whose surface samples yielded a weighted mean CRE age of 175 ± 62 ka. Assuming 175 ka represents the actual age of T2 tread and subtracting the concentration acquired *in situ*, at 2.1 m depth, by sample DS08P130 during these 175 ka of exposure would yield to a remaining, hence inherited, concentration of $7.25 \cdot 10^5$ at.g⁻¹(SiO₂). Most of the sample concentration would therefore result from inheritance. Such inherited concentration would have been acquired in about 60 ka, if accumulated at the surface. Then, the 70 ka ages of riverbed samples appear to give a good estimate of the amount of inheritance carried by T2 material. Consequently, T2 mean age should be reduced to 105 ± 62 ka. These 70 ka inheritance estimates are larger than the 32 ka of inheritance age-equivalent obtained for T3 by conventional modelling of the ¹⁰Be profile (Figure 9). We have therefore investigated another method to use the inheritance. Assuming each terrace formed during a short-lived aggradation coeval with a single climatic crisis, the near-surface concentrations have been used to fix the maximum abandonment age of the terrace (Figure 14). The principle is simple and rests on the impossibility for any sample to be incorporated into the sediment of the terrace with a negative concentration. Accounting for the depth of each near-surface sample and assuming its measured concentration results only from *in-situ*

550 exposure; i.e. assuming no inheritance for the sample, it is possible to calculate for any
551 sample of a profile the time required to bring it back from its measured concentration to a null
552 concentration. The maximum abandonment age of the terrace is then obtained from the near-
553 surface sample of a given profile for which the concentration is restored to zero without
554 bringing back any other sample of the profile to a negative concentration. For the profile PS1
555 across T2 (Figure 14a), this is obtained for the sample DS08P127 with 107 ka of *in-situ*
556 exposure. This indicates that T2 was abandoned at most 107 ka ago and that for this
557 maximum time of exposure the concentration remaining in the other samples of the profile
558 correspond to a minimum inheritance. Therefore, this method figures out the variability of the
559 inheritance that amounts, for such an exposure time, to $7.86 \cdot 10^5 \text{ at.g}^{-1}(\text{SiO}_2)$ for the near-
560 surface amalgam collected at 2.1 m depth; such concentration would correspond to a
561 minimum exposure of 66 ka if acquired at the surface prior to the emplacement of the terrace
562 (Figure 14a). It is worth noticing that this rejuvenation would bring back only one of the
563 surface samples to a negative concentration. This remains acceptable, as this sample is the
564 statistical outlier DS08S114. All the other such 107 ka-rejuvenated surface samples would
565 keep positive concentrations. While older depth-profile determined CRE ages of T2 are not
566 possible because they would bring, at least one of the near-surface amalgams, the amalgam
567 127 (Figure 14a), back to a negative concentration, younger exposure ages remain possible.
568 Theoretically, all exposure ages ranging between 0 and 107 ka are possible. On the one hand,
569 exposure ages ranging between 53 ka (oldest possible age of the youngest sample, DS08S114,
570 on T2) and 107 ka would make that statistical outlier younger than the age of the terrace. On
571 the other hand, exposure ages ranging between zero and 53 ka would be compatible with the
572 occurrence of the statistical outlier as well as the other surface samples collected on T2.

573 The same method applied to the depth profile PN across T3 (Figure 14b) demonstrates
574 the terrace was abandoned at most 412 ka ago, confirms the occurrence of a significant
575 inheritance which minimum amounts to 68 ka for the deepest amalgam collected at more than
576 3m depth, and exemplifies its variability. It is nonetheless important to notice that this is an
577 uppermost bound of exposure duration. This leaves open all the possibilities ranging between
578 the time of abandonment of T2 and 412 ka, hence at least the possibilities between 107 and
579 412ka.

580

581 3.4.2 Abandonment age of terrace treads.

582 The age of abandonment of the uppermost level T3 is to be discussed with the only
583 data available, the CRE ages (Figures 13 and 15). One may rest on the statistical analysis of

584 the surface samples and retains the weighted mean age of 469 ± 88 ka. To account for the
585 inheritance incorporated in the former estimate, it is possible to subtract to that weighted
586 mean age the 32 ka of inheritance age-equivalent obtained from the modelling of the ^{10}Be
587 profile. It is nonetheless worth noticing that this average inheritance has been modelled under
588 the incorrect assumption that the inheritance is homogeneous. Accounting for the variability
589 of the inheritance, the near-surface profile data are incompatible with an age older than 412 ka
590 (Figure 14b) and the large uncertainties of the former estimate (437 ± 88 ka) can be reduced
591 to the interval 349-412 ka (Figure 15). Alternatively, retaining the youngest sample and
592 allowing for the occurrence of a greater amount of inheritance would provide a much younger
593 abandonment age of 271 ka (oldest possible CRE age of the youngest sample). As there is
594 ample evidence for a large variability of the inheritance on the younger surfaces, one cannot
595 rule out the later hypothesis and may consider an age of 271 ka for the abandonment of T3.

596 The age of abandonment of the intermediate level T2 is easier to estimate because both
597 OSL and CRE ages are available. The weighted mean of the zero-erosion CRE age (175 ± 62
598 ka) is of little use for constraining the age of abandonment because of the variable inheritance.
599 Subtracting a possible inheritance of 70 ka (Figure 14a), a value similar to the average
600 obtained for the cobbles collected in the active riverbed, takes back the former estimate to 105
601 ± 62 ka. Although limiting the uncertainties to the range 43 -107 ka, the upper bound on the
602 abandonment age (Figure 14a) allows for a wide range of possibilities, including the oldest
603 possible CRE age (53 ka) of the youngest surface cobble. Accounting for the occurrence of a
604 variable inheritance, this latter solution is a better estimate of the maximum age of
605 abandonment of the surface although the youngest cobble may also bear an inherited
606 component. This inherited component may correspond to the difference with the oldest
607 possible age of the youngest OSL collected below the tread of T2. The surface of T2 is
608 younger than the oldest possible age of the superficial OSL sample and is at most 28.2 ka at
609 site Dehshir South (Figure 13b). Assuming this OSL age is close to the actual abandonment
610 age of T2 tread, a forward modelling of near-surface concentrations of PS1 profile (fig 11c)
611 can be calculated with zero erosion and different choices of inheritance. Whatever the
612 selected value of homogeneous inheritance, none permits to account correctly for the uneven
613 distribution with depth of the measured near-surface concentrations. Nevertheless, two
614 limiting curves appear to bracket these measured concentrations, they correspond to $3.5 \cdot 10^5$
615 and $9 \cdot 10^5$ $\text{at.g}^{-1}(\text{SiO}_2)$ of homogeneous inheritances (figure 11c). These values of inherited
616 concentrations would correspond to pre-exposure, if acquired at the surface prior to the
617 emplacement of the terrace, of 30 ka and 75 ka, respectively. Although these values of

618 inherited concentrations result from forward modelling based on the assumption that the
619 inheritance is homogeneous, they indicate the inheritances carried by the amalgam samples of
620 T2 sediments may be nearly as high as 10^6 at.g⁻¹(SiO₂). It is worth noticing that all but one
621 measured surface samples have ¹⁰Be concentrations that are higher than 10^6 at.g⁻¹(SiO₂).
622 Interestingly, subtracting to the near-surface samples the concentrations corresponding to 30
623 ka of *in-situ* exposure makes the residual concentrations, which correspond to inheritance,
624 noteworthy. This inherited concentration amounts to $8.57 \cdot 10^5$ at.g⁻¹(SiO₂) for sample
625 DS08P130 at 2.1 m depth and corresponds to pre-exposure time at the surface of 71 ka. Thus
626 considering 70 ka of inheritance for T2 gravels is a reasonable estimate that can be proposed
627 to average the variable inheritance.

628 Finally, the OSL ages of the risers T1b/T0 and T1a/T0 indicates their respective tread
629 are at most 23.4 ka and 10.6 ka, respectively. Given the uncertainties associated to the OSL
630 ages of the risers and considering that partial bleaching has been accounted, the youngest
631 possible ages of T2, T1b, and T1a treads are respectively 25.6 ka, 20.4 ka, and 9.4 ka.

632

633

4. Slip-rate estimate and conclusions

634 The former chronology and offset-risers provide estimates on the minimum and
635 maximum slip-rate of the Dehshir fault. At site Dehshir South, the river course displaced by
636 380 ± 20 m is incised within the terrace T3. Combining the offset of 380 ± 20 m with the
637 maximum exposure age of 412 ka yields a minimum slip-rate of 0.92 ± 0.05 mm.yr⁻¹.
638 Assuming that the regional level T3 is coeval at both sites and that the oldest possible age of
639 the youngest sample collected on T3 (i.e., 271 ka) may approximate its abandonment, the slip-
640 rate would be at least 1.40 ± 0.08 mm.yr⁻¹. The 25m-deflection of the Marvast River might
641 also be used to estimate the slip-rate on a shorter period of time, but this deflection probably
642 overestimates the true tectonic offset because T1 tread is no longer observed downstream. The
643 offset of the gullies incising both T3 and T2 treads at site Dehshir North is a true tectonic
644 offset. This 20-30m offset provides reliable estimates of the upper and lower bounds of the
645 slip-rate. The offset cannot be older than the OSL age collected below the tread of T2 (OSL1
646 26.9 ± 1.3 ka) and accounts for a minimum slip-rate greater than 0.71 mm.yr⁻¹ (20 m in the
647 last 28.2 ka). The offset cannot be younger than the infilling of T1b and allows determining
648 the upper and lower bounds of the maximum slip-rate. The infilling of T1b being younger
649 than 21.9 ± 1.5 ka, the lower and upper bounds of the maximum slip-rate are respectively 0.85
650 mm.yr⁻¹ (20 m in the last 23.4 ka) and 1.47 mm.yr⁻¹ (30 m in the last 20.4 ka). The 12 ± 2 m-

651 offset of the riser T1a/T0 at Dehshir North is also an estimate of the actual tectonic offset
652 postdating the emplacement of T1a, which is at most 10.6 ka according to sample OSL IV
653 (Table 3, Figure 13). The 12 ± 2 m-offset yields a lower bound of the minimum slip-rate of
654 1.13 ± 0.2 mm.yr⁻¹. The early estimate of Nazari et al. (2009) can therefore be refined and the
655 actual slip rate ranges between 0.93 mm.yr⁻¹, largest of the conservative estimates of the
656 minimum slip rate, and 1.47 mm.yr⁻¹, safe estimate of the maximum slip rate. Therefore, the
657 slip-rate of the Dehshir fault is well determined at 1.2 ± 0.3 mm.yr⁻¹ (Figure 15).

658 This study demonstrates the usefulness of combining CRE and OSL data to unravel
659 the abandonment ages of alluvial fans and inset terraces in the desert environment of Central
660 Iran. On the one hand, the use of ¹⁰Be and ³⁶Cl cosmogenic isotopes with different half-lives
661 allows constraining a very low denudation-rate of 0.001 mm.yr⁻¹ for the terrace treads and
662 alluvial fan surfaces of Central Iran. On the other hand, the combination of surface and near-
663 surface sampling exemplifies the occurrence and the variability of inheritance in the
664 cosmogenic isotope concentrations and emphasizes the difficulty in assessing abandonment
665 ages of young alluvial surfaces with CRE measurements in such arid environment (e.g., Le
666 Dortz et al., 2009). The scattering of the CRE surface and near-surface concentrations
667 indicates that the cobbles have not been uniformly exposed to cosmic rays prior to their
668 emplacement. This variable inheritance may originate from a differential exhumation and
669 weathering of the bedrock catchments, or more likely for Dehshir sites, from reworking of
670 cobbles originating from different levels of upper, hence older, fans. The abandonment age of
671 an alluvial surface is thus better estimated by the CRE age of the youngest surface sample
672 than by the weighted mean CRE age of many samples, as already formulated in Mongolia
673 (Vassalo et al., 2007) and along the southern rim of the Tarim basin (Mériaux et al., 2005).
674 However, the youngest sample on a surface may also incorporate inheritance and still
675 overestimate the abandonment age. The amount of CRE inheritance potentially remaining in
676 the youngest sample of a given surface may be obtained by comparing with the OSL age of
677 the late sediments aggraded before the abandonment of the surface. For alluvial surfaces that
678 are young with respect to the considerable amount of inheritance, up to 70 ka in the desert
679 environment of Central Iran, the upper bound on the abandonment age of an alluvial surface
680 appears best estimated by the OSL dating of the late sediment aggraded. For such young
681 surfaces, the CRE measurements are complementary of OSL dating and can be used to
682 unravel the complex history of weathering and transport in the catchment of desert alluvial

683 fans. Finally, such variable CRE inheritance, typifying arid endorheic regions without incision
684 rates, may require more consideration than hitherto drawn for the Andes and Tibet plateaus.

685

686 **Acknowledgments.**

687 This study would have been impossible without financial assistance from INSU-CNRS
688 (PNTS and 3F programs) and CNES-SPOT Image (ISIS program contracts ISIS0403-622 and
689 ISIS0510-812). Université Pierre et Marie Curie (UPMC) and Geological survey of Iran
690 (GSI) provided complementary funding and logistic assistance. KL received a Ministry of
691 Research and Education scholarship granted by the President of UPMC. The ^{10}Be
692 measurements were performed at the ASTER AMS national facility (CEREGE, Aix en
693 Provence) that is supported by the INSU/CNRS, the French Ministry of Research and Higher
694 Education, IRD and CEA. The ^{36}Cl measurements were performed at the LLNL-CAMS. We
695 thank L. Leanni, K. Pou, B. Finkel, F. Chauvet, M. Arnold and G. Aumaître for their help
696 during chemistry and measurements at CEREGE and acknowledge B. Oveisi and M.
697 Nazemzadeh for efficient organization and help during fieldwork. We acknowledge thorough
698 reviews by Richard Walker and Anne-Sophie Mériaux. We are very thankful to Anne-Sophie
699 Mériaux for her acute verification of the cosmogenic calculations.

700

701

702

References

- 703 Anderson, R.S., J.L. Repka and G.S. Dick., 1996. Explicit treatment of inheritance in dating
704 depositional surfaces using in situ ^{10}Be and ^{26}Al , *Geology*, **24**, 47–51.
- 705 Arnold M., Merchel S., Bourles D.L., Braucher R., Benedetti L., Finkel R.C., Aumaître G.,
706 Gottdang A. & Klein M., 2010. The French accelerator mass spectrometry facility
707 ASTER: Improved performance and developments. *Nuclear Instruments and*
708 *Methods in Physics Research B*, **268**: 1954–1959.
- 709 Bateman, M.D., Boulter, C.H., Carr, A.S., Frederick, C.D., Peter, D. and Wilder, M., 2007.
710 Detecting Post-depositional sediment disturbance in sandy deposits using optical
711 luminescence. *Quaternary Geochronology*, **2(1-4)**, 57-64.
- 712 Berberian, M., 1981. Active faulting and tectonics of Iran, in Zagros, Hindu Kush, Himalaya:
713 geodynamic evolution, *Geodyn. Ser.*, **3**, eds Gupta, H.K. & Delany, F.M., 33–69.
- 714 Boulter, C., Bateman, M.D. and Frederick, C.D., 2007. Developing a protocol for selecting
715 and dating sandy sites in East Central Texas: Preliminary results. *Quaternary*
716 *Geochronology* **2**, 45-50.

- 717 Braucher R., Brown E.T., Bourle's D.L., Colin F., 2003. In situ produced ^{10}Be measurements
718 at great depths: implications for production rates by fast muons. *Earth Planet., Sci.*
719 *Lett.*, **211**, 251-258.
- 720 Braucher, R., P. Del Castillo, L. Siame , A.J. Hidy , D.L. Bourlès., 2009. Determination of
721 both exposure time and denudation rate from an in situ-produced ^{10}Be depth profile :
722 A mathematical proof of uniqueness. Model sensitivity and applications to natural
723 cases. *Quaternary Geochronology* **Volume 4**, Issue 1, Pages 1-82
- 724 Brown, E. T., J. M. Edmond, G. M. Raisbeck, F. Yiou, M. D. Kurz, and E. J. Brook, 1991.
725 Examination of surface exposure ages of Antarctic moraines using in situ produced
726 ^{10}Be and ^{26}Al , *Geochim. Cosmochim. Acta*, **55**, 2699 – 2703.
- 727 Brown, E.T., Bourlès, D.L., Raisbeck, G.M., Yiou, F., Burchfiel, B.C., Molnar, P., Deng, Q.,
728 Li, J., 1998. Estimation of slip rates in the southern Tien Shan using cosmic ray
729 exposure dates of abandoned alluvial fans. *Geol. Soc. Am. Bull.* **110** (3), 377–386.
- 730 Chmeleff, J., von Blackenburg, F., Kossert, K., Jakob, D., 2010. Determination of the ^{10}Be
731 half-life by multicollector ICP-MS and liquid scintillation counting. *Nuclear*
732 *Instruments and Methods in Physics Research B*, **268**, 192–199.
- 733 DeLong, S.B., Arnold, L.J., 2007. Dating alluvial deposits with optically stimulated
734 luminescence, AMS ^{14}C and cosmogenic techniques, western Transverse Ranges,
735 California, USA. *Quat. Geochron.* **2**, 129–136.
- 736 Desilets, D., Zreda, M., Almasi, P.F., Elmore, D., 2006. Determination of cosmogenic ^{36}Cl in
737 rocks by isotope dilution: innovations, validation and error propagation. *Chemical*
738 *Geology* **233**, 185-195.
- 739 Farber, D., Meriaux, A-S., Finkel, R., 2008. Attenuation length for fast nucleon production of
740 ^{10}Be derived from near-surface production profiles. *Earth and Planetary Science*
741 *Letters* **274**, 295-300.
- 742 Fattahi, M., Walker, R., Hollingsworth, J., Bahroudi, A., Talebian, M., Armitage, S. and
743 Stokes, S., 2006. Holocene slip-rate on the Sabzevar thrust fault, NE Iran,
744 determined using Optically-stimulated Luminescence (OSL). *Earth and Planetary*
745 *Science Letters*, **245**: 673-684.
- 746 Fattahi, M., Walker, R., Khatib, M.M., Dolati, A. and Bahroudi, J., 2007. Slip-rate estimates
747 and past earthquakes on the Doruneh fault, eastern Iran. *Geophysical Journal*
748 *International*, **168**: 691-709
- 749 Fattahi, M., Nazari, H., Bateman, M.D., Meyer, B., Sébrier, M., Talebian, M., Le Dortz, K.,

- 750 Foroutan, M., Ahmadi Givi, F. and Ghorashi, M., 2010. Refining the OSL age of the
751 last earthquake on the Dheshir fault, Central Iran. *Quat. Geochronology*. **5**, 286–292,
752 Doi:10.1016/j.quageo. 2009.04.005.
- 753 Galbraith, R. F., Roberts, R.G., Laslett, G.M., Yoshida H., Olley, J.M., 1999. Optical dating
754 of single and multiple grains of quartz from Jinmium rock shelter, northern Australia,
755 part 1, Experimental design and statistical models. *Archaeometry* **41**, 339-364.
- 756 Gosse, J.C., Phillips, F.M, 2001. Terrestrial in situ cosmogenic nuclides: theory and
757 application. *Quaternary Science Reviews* **20**, 1475-1560.
- 758 Geological Survey of Iran, 1981. Geological Map of Iran, Ministry of Industry and Mines,
759 scale 1:250 000, Anar quadrangle map.
- 760 Hetzel, R., Tao, M., Stokes, S., Niedermann, S., Ivy-Ochs, S., Gao, B., Strecker, M.R., Kubik,
761 P.W., 2004. Late Pleistocene/Holocene slip rate of the Zhangye thrust (Qilian Shan,
762 China) and implications for the active growth of the northeastern Tibetan Plateau.
763 *Tectonics* **23** (6), TC6006, doi:10.1029/2004TC001653.
- 764 Korschinek, G., Bergmaier, A., Faestermann, T., Gerstmann, U. C., Knie, K., Rugel, G.,
765 Wallner, A., Dillmann, I., Dollinger, G., Lierse von Gosstomski, Ch., Kossert, K.,
766 Maiti, M., Poutivtsev, M., Remmert, A., 2010. A new value for the ^{10}Be half-life by
767 Heavy-Ion Elastic Recoil detection and liquid scintillation counting. *Nuclear*
768 *Instruments and Methods in Physics Research B*, **268**, 187–191.
- 769 Le Dortz, K., Meyer, B., Sebrier, M., Nazari, H., Braucher, R., Fattahi, M., Benedetti, L.,
770 Foroutan, M., Siame, L., Bourles, D., Talebian, M., Bateman, M.D. and Ghorashi,
771 M., 2009. Holocene right-slip rate determined by cosmogenic and OSL dating on the
772 Anar fault, Central Iran. *Geophys. J. Int.*, **179**, 700–710 Doi:10.1111/j.1365-
773 246X.2009.04309.x.
- 774 Matmon, O., Simhai, R. Amit, I. Haviv, Y. Enzel, N. Porat, E.V. McDonald, L. Benedetti and
775 R.C. Finkel, 2009. Desert pavement-coated surfaces in extreme deserts present the
776 longest-lived landforms on Earth, *Geol. Soc. Am. Bull.* **121**, pp. 688–697.
- 777 Merchel S. & Herpers U., 1999. An update on radiochemical separation techniques for the
778 determination of long-lived radionuclides via accelerator mass spectrometry.
779 *Radiochimica Acta*, **84**: 215-219.
- 780 Merchel S., Arnold M., Aumaître G., Benedetti L., Bourles D.L., Braucher R., Alfimov V.,
781 S.P.H.T. Freeman, Steier P. & Wallner A., 2008. Towards more precise ^{10}Be and ^{36}Cl

- 782 data from measurements at the 10-14 level: Influence of sample preparation. *Nuclear*
783 *Instruments and Methods in Physics Research B*, **266**: 4921-4926.
- 784 Mériaux, A.-S., Tapponnier, P. Ryerson, F. J. Xiwei, X. King, G. Van der Woerd, J. Finkel,
785 R. C. Haibing, L. Caffee, M. W. Zhiqin, X., 2005. The Aksay segment of the
786 northern Altyn Tagh fault: Tectonic geomorphology, landscape evolution, and
787 Holocene slip rate, *J. Geophys. Res.*, **110**, B04404
- 788 Meyer, B., Mouthereau, F., Lacombe, O. & Agard, P., 2006. Evidence of quaternary activity
789 along the Deshir Fault, *Geophys. J. int.*, **164**, 192-201.
- 790 Meyer, B. and K. Le Dortz, 2007. Strike-slip kinematics in Central and Eastern Iran :
791 estimating fault slip-rates averaged over the Holocene. *Tectonics*, **6**, TC5009,
792 doi:10.1029/2006TC002073, 2007.
- 793 Murray, A.S. and A.G. Wintle, 2000. Luminescence dating of quartz using an improved
794 single-aliquot regenerative-dose protocol, *Radiation Measurements*, **32**, 57-73.
- 795 Nazari, H., M. Fattahi, B. Meyer, M. Sébrier, M. Talebian, M. Foroutan, K. Le Dortz, M. D.
796 Bateman and M. Ghorashi, 2009. First evidence for large earthquakes on the Deshir
797 fault, Central Iran Plateau. *Terra Nova*, **21**, 417–426.
- 798 Nissen, E., Walker R.T., Bayasgalan B., Carter A, Fattahi M., Molor E., Schnabel C., West A.
799 J., Xu S., 2009. The late Quaternary slip-rate of the Har-Us-Nuur fault (Mongolian
800 Altai) from cosmogenic ¹⁰Be and luminescence dating, *Earth Planet. Sci. Lett.*
801 doi:10.1016/j.epsl.2009.06.048
- 802 Owen, L.A., R.C. Finkel, H. Ma, J.Q. Spencer, E. Derbyshire, P. Banard and M.W. Caffee.,
803 2003. Timing and style of late Quaternary glaciation in northeastern Tibet,
804 *Geological Society of America Bulletin* **115**, pp. 1356–1364
- 805 Owen, L.A., Finkel, R.C., Haizhou, M., Barnard, P.M., 2006. Late Quaternary landscape
806 evolution in the Kunlun Mountains and Qaidam Basin, Northern Tibet: a framework
807 for examining the links between glaciation, lake level changes and alluvial fan
808 formation. *Quat. Int.* **154–155**, 73–86.
- 809 Repka, J.L., Anderson, R.S., Finkel, R.C., 1997. Cosmogenic dating of fluvial terraces,
810 Fremont River, Utah. *Earth Planet. Sci. Lett.* **152**, 59–73.
- 811 Roberts, R.G., R.F. Galbraith, H. Yoshida, G.M. Laslett, J.M. Olley, 2000. Distinguishing
812 dose populations in sediment mixtures: a test of single-grain optical dating
813 procedures using mixtures of laboratory-dosed quartz. *Radiation Measurements* **32** ,
814 459-465
- 815 Schimmelpfennig, I., Benedetti, L., Finkel, R., Pik, R., Blard, P-H., Bourlès, D., Burnard, P.,

- 816 Williams, A., 2009. Sources of in-situ ^{36}Cl in basaltic rocks. Implications for
817 calibration of production rates. *Quaternary Geochronology*, vol **4**, issue 6, 441-461.
- 818 Siame, L., O. Bellier, R. Braucher, M. Sebrier, M. Cushing, D. Bourlès, B. Hamelin, E.
819 Baroux, B. de Voogd, G. Raisbeck, F. Yiou, 2004. Local erosion rates versus active
820 tectonics : cosmic ray exposure modelling in Provence (south-east France). *Earth*
821 *Planet. Sci. Lett.*, **220**, 3-4, 345-364,
- 822 Stone, J. O. H., Allan, G. L., Fifield, L. K., Cresswell, R. G., 1996. Cosmogenic chlorine-36
823 from calcium spallation, *Geochim. Cosmochim. Acta*, **60**, 679-692.
- 824 Stone, J. O., Evans, J. M., Fifield, L. K., Allan, G. L., Cresswell, R. G., 1998. Cosmogenic
825 chlorine-36 production in calcite by muons, *Geochim. Cosmochim. Acta*, **62**, 433-
826 454.
- 827 Stone J. O., 2000. Air pressure and cosmogenic isotope production. *J. Geophys. Res.*, **105**,
828 B10, 23753-23759.
- 829 Vassallo R, Ritz J, F., Braucher R, Jolivet M, Carretier S, Larroque C, Chauvet A, C. Sue C,
830 Todbileg M, Bourlès D, Arzhannikova A, Arzhannikov S., 2007. Transpressional
831 tectonics and stream terraces of the Gobi-Altay, Mongolia. *Tectonics* **26**, TC5013,
832 doi:10.1029/2006TC002081.
- 833 Vermeesch, P., 2007. CosmoCalc: An Excel add-in for cosmogenic nuclide calculations,
834 *Geochem. Geophys. Geosyst.*, **8**, Q08003, doi:10.1029/2006GC001530.
- 835 Walker, R. and J. Jackson, 2004. Active tectonics and late Cenozoic strain distribution in
836 central and eastern Iran, *Tectonics*, **23**, TC5010, doi:10.1029/2003TC001529.
- 837 Zreda, M. G., Philips, F. M., Elmore, D., Kubik, P. W., Sharma, P., Dorn, R. I., 1991.
838 Cosmogenic chlorine-36 production rates in terrestrial rocks, *Earth Planet. Sci. Lett.*,
839 **105**, 94-109.
- 840

840 Figures captions

841

842 Figure1: Spot imagery of the southern part of the Dehshir fault, near Marvast town. The fault
843 cuts across abandoned alluvial fan systems and active rivers. Boxes indicate locations of
844 Figures 2 and 4. The inset is a Landsat mosaic of the Dehshir fault and surroundings. The
845 Nain Baft ophiolite outcrops are stylized in purple. The total dextral offset of the fault ($65 \pm$
846 15 km) is outlined by the displacement of the suture.

847

848 Figure 2: Site Dehshir South. a) Quickbird imagery. The fault trace cuts across the Marvast
849 River, intermittent channels and successive abandoned fans and terraces (T3 in orange, T2 in
850 yellow, T1 a and b in green). The numbered dots show the position of the surface samples
851 collected for ^{10}Be and ^{36}Cl CRE dating (red and blue dots, respectively). The black squares
852 show the position of the near-surface samples collected along depth profiles PS1 and PS2
853 (Figure 11, 12 and 13). The black dots locate the OSL samples taken below the ground
854 surface. AB locates the topographic profile of figure 3. b) Close up on the $380 \pm 20\text{m}$ dextral
855 offset of a river course, incised within the oldest (T3) fan surface.

856

857 Figure 3: a) Topographic profile across the abandoned fan system (see location on figure 2)
858 highlights the relative elevation of the terraces and their degree of incision by the Marvast
859 river. The profile is work out from a differential GPS survey. b) Field photograph of the inset
860 terraces. Location of OSL III and IV are indicated on the close up pictures of the risers
861 T1b/T0 and T1a/T0 respectively.

862

863 Figure 4: Site Dehshir North. a) Quickbird imagery. Different coloured shading denotes the
864 successive abandoned fans (same code as for Figure 2). Numbered dots show the position of
865 the surface samples collected for ^{10}Be and ^{36}Cl CRE dating (red and blue dots, respectively).
866 The black square shows the position of the near-surface samples collected along the depth
867 profiles PN (Figure 7 and 8). The black dots locate the OSL samples taken below the ground
868 surface. Rectangle denotes the close up on the offset riser on figure 5. Dotted circles indicate
869 location of 20-30 m right-lateral offset-gullies. Black (AB and CD) and white (RI) lines locate
870 topographic sections on each side of the fault and on the riverbed respectively. b)
871 Topographic profiles, achieved from differential GPS survey and projected along fault strike,
872 highlight the amount of stream incision upstream and down stream of the fault. The offset-
873 gullies are indicated.

874

875 Figure 5: a) Raw (left panel) and interpreted (right panel) images of the dextral offset of the
876 recent riser (T1a/T0). Open triangles point to the fault trace and arrows to the foot of the riser.
877 Rectangle denotes the enlargement on the offset-riser b) Quickbird image wrapped on the
878 digital elevation model worked out from a DGPS survey. c) Enlargement on the 12 ± 2 m
879 offset-riser (T1a/T0 downstream, T3/T0 upstream). The blue line denotes the base of the riser.
880 d) Field photograph of the offset-riser with vertical arrows pointing to the foot of the riser.

881

882 Figure 6: Summary of observations at site Dehshir North. a) ^{10}Be and ^{36}Cl CRE ages of
883 surface samples modelled without erosion and without inheritance are indicated by red and
884 blue dots above each surface. The shaded columns extend from the minimum age to the
885 maximum age given by the error bars of the samples. The OSL samples collected beneath
886 each surface are indicated in stratigraphic order (see text for discussion). The plot of CRE
887 ages is given for each surface sample, in relative position from north to south. Dots and errors
888 bars are in red and blue for ^{10}Be and ^{36}Cl , respectively. b) Distribution of *in-situ* produced ^{10}Be
889 (left panel) and ^{36}Cl (right panel) CRE ages modelled without erosion and without inheritance
890 for the surface samples collected on T3 tread. The thin curves represent the CRE age
891 probability as Gaussian distribution for each individual sample and the thick curves
892 correspond to the summed Gaussian density probability function. The weighted mean CRE
893 age is obtained with errors equal to two standard deviations (2σ). Outlier sample DN06S2
894 (235.5 ± 35.4 ka) has not been included in the ^{10}Be statistics.

895

896 Figure 7: Summary of observations at site Dehshir South. a) ^{10}Be and ^{36}Cl CRE ages of
897 surface samples modelled without erosion and without inheritance are indicated by red and
898 blue dots above each surface. The shaded columns extend from the minimum age to the
899 maximum age given by the error bars of the samples. The OSL samples collected beneath
900 each surface are indicated in stratigraphic order (see text for discussion). The plot of CRE
901 ages is given for each surface sample, in relative position from north to south. Dots and errors
902 bars are in red and blue for ^{10}Be and ^{36}Cl , respectively. b) Distribution of *in situ* produced ^{10}Be
903 (left) and ^{36}Cl (right) CRE ages modelled without erosion and without inheritance for the
904 surface samples collected on T3 Tread. The thin curves represent the CRE age probability as
905 Gaussian distribution for each individual sample and the thick curves correspond to the

906 summed Gaussian density probability function. The weighted mean age is obtained with
907 errors equal to two standard deviations (2σ).

908

909 Figure 8: Plot of the near-surface, measured ^{36}Cl concentrations (black dots) as a function of
910 depth at profile PN (location on figure 4). Surface samples (blue dots) are shown but not
911 included in the modelling. The erosion rate is modelled for a 3 Ma-old surface to ensure that
912 the steady state equilibrium between production and disintegration has been reached. For the
913 three different densities tested (obtained from the near-surface samples), the best-fit erosion
914 rate – inheritance is indicated.

915

916 Figure 9. a) Plot of the near-surface, measured ^{10}Be concentrations (black dots) as a function
917 of depth at profile PN (location on figure 4). Surface samples are indicated as red dots. The
918 modelled curves fit distributions of concentrations, without erosion, and for three assigned
919 inheritances. The modelling includes both the near-surface samples and the weighted mean
920 age of the surface samples (DN06S2 excluded). b) $\text{Log}(\chi^2)$ values for a range of inheritance
921 and CRE ages modelled without erosion are plotted below. The modelling converges towards
922 a best-fit age of 460 ka and inheritance $3.8 \cdot 10^5 \text{ at.g}^{-1}(\text{SiO}_2)$ (star).

923

924 Figure 10: Weighted mean ^{10}Be CRE age of T3 tread including the surface sample exposure
925 ages of North and South sites and excluding outlier sample DN06S2. The thin curves
926 represent the CRE age probability as Gaussian distribution for each individual sample and the
927 thick curves correspond to the summed Gaussian density probability function. The weighted
928 mean age is obtained with errors equal to two standard deviations (2σ).

929

930 Figure 11: a) Weighted mean CRE age for the ^{10}Be and ^{36}Cl surface samples collected on T2
931 tread at Dehshir South site. The ages have been calculated assuming no erosion and no
932 inheritance and the sample DS08S114 ($49.9 \pm 3.3 \text{ ka}$) has not been included in the statistics.
933 The thin curves represent the CRE age probability as Gaussian distribution for each individual
934 sample and the thick curves correspond to the summed Gaussian density probability function.
935 The weighted mean age is obtained with errors equal to two standard deviations (2σ). b)
936 Field photograph showing the 4m high T2/T0 riser sampled for profile PS1 (see Figure 2 for
937 location). c) Profile of ^{10}Be concentrations through the terrace T2 at site PS1. Red and blue
938 dots are surface and near-surface samples, respectively. The two OSL samples collected by

939 the same riser along strike within sandy lenses are indicated. Dashed curves represent the
940 forward models of theoretical ^{10}Be near-surface concentration for a 30 ka abandonment age
941 assuming homogeneous inheritances of $3.5 \cdot 10^5 \text{ at.g}^{-1}(\text{SiO}_2)$ (left) and $9 \cdot 10^5 \text{ at.g}^{-1}(\text{SiO}_2)$ (right).

942

943 Figure 12: Plot of the measured ^{10}Be concentrations as a function of depth (left panel) and
944 simplified stratigraphy (right panel) through profile PS2. Depth profile PS2 has been
945 excavated within T2 tread, North of the Marvast River (see location on figure 2). Relative
946 positions of OSL samples AB/2006/I and II and CRE near-surface amalgams are shown
947 (blacks arrows).

948

949 Figure 13: Synthesis of observations and plot of sample ages in relative position from north to
950 south for site Dehshir North (left panels) and site Dehshir South (right panels). Dots and
951 errors bars are in red, blue and black for ^{10}Be , ^{36}Cl and OSL dating, respectively. a) The thick
952 lines and shaded regions are the weighted mean with 2σ confidence interval for the CRE
953 surface age. Samples DN06S2 and DN08S114 have been omitted for the T3 and T2 statistics,
954 respectively. The thin lines are the oldest possible CRE age of the youngest CRE sample
955 collected on the terrace treads. b) Upper part, relative positions and OSL ages of the samples
956 collected below the terrace treads of T2, T1b and T1a. Samples HI (Nazari et al., 2009;
957 Fattahi et al., 2010) and AB have been collected within trenches excavated for paleoseismic
958 purposes and samples OSL I-IV by the terrace risers. Lower part, CRE and OSL ages
959 available for terraces T2 and T1. The thick black line is the oldest possible age of the most
960 surficial OSL sample collected below each terrace tread.

961

962 Figure 14: Depth-profile PS1 and PN of ^{10}Be concentrations respectively through terrace T2
963 (a) and T3 (b). Violet and red dots are the measured concentrations of the near-surface
964 amalgams and surface samples, respectively. Blue dots and black dots are the respective
965 concentrations of the near-surface amalgams and surface samples once one near-surface
966 amalgam is restored to a null concentration without bringing back any other near-surface
967 sample to a negative concentration (see text for discussion). The time of *in-situ* exposure to
968 bring that near-surface sample to its measured concentration is indicated in red, and the
969 residual concentrations remaining in the other near-surface samples by black arrows
970 materializing the sample inheritance for such duration of exposure. The only rejuvenated
971 surface sample displaying a negative concentration is the sample DN06S2 on T3, therefore a

972 statistical and physical outlier for a 412 ka exposure age. This race to zero-concentration for
973 the near-surface amalgams indicates that T2 and T3 have to be younger than 107 ka and 412
974 ka, respectively. Shaded area corresponds to physically unrealistic domains of negative ^{10}Be
975 concentrations.

976

977 Figure 15: Summary of offsets and ages available to assess the slip-rate of the Dehshir fault.
978 Dashed boxes and boxes correspond to weighted mean CRE age with and without removal of
979 the estimated inheritance (see text for discussion). The oldest possible abandonment ages of
980 T3 and T2 (thick vertical black lines) are determined from the near-surface concentrations
981 (Figure 14). The exposure age of the youngest sample (black cross) on each terrace is also
982 indicated. Grey boxes correspond to the OSL age domains of the late sediments emplaced
983 below the treads of T2 and T1. Light grey slip-rate domain is the range of minimum slip-rate
984 of Nazari et al. (2009). The dark grey domain narrows the uncertainties and demonstrates the
985 Dehshir fault slips faster than 0.93 mm.yr^{-1} but slower than 1.47 mm.yr^{-1} .

986

987 Table 1: The ^{10}Be and ^{36}Cl nuclide concentrations and CRE modelled ages for surface and
988 near-surface samples along the Dehshir fault. Propagated analytical uncertainties include error
989 blank, carrier and counting statistics. Zero erosion model ages are calculated for surface
990 samples with propagated analytical uncertainties, including error blank, carrier and counting
991 statistic; corresponding geographic correction factors and without shielding in agreement with
992 site topography. ^{10}Be and ^{36}Cl half-life are respectively 1.387 Ma (Chmeleff et al., 2010;
993 Korshincek et al., 2010) and 301 ka (Gosse & Philipps, 2001). For surface samples, a density
994 of 2.2 g.cm^{-3} and 2 g.cm^{-3} have been used for quartz and carbonates samples respectively. An
995 attenuation length of 160 g.cm^{-2} (Gosse & Philipps, 2001) has been used. Stone (2000)
996 polynomial has been used to determine surficial production rate assuming a SLHL production
997 rate of $4.49 \text{ at.g}^{-1}.\text{yr}^{-1}$ for ^{10}Be with 6% of uncertainty. The ^{36}Cl production rate of 48.8 ± 3.4
998 $\text{at.g}^{-1}.\text{yr}^{-1}$ is from Stone (1996). ^{10}Be ages have been calculated using Cosmocalc (Vermeesh
999 2007). ^{36}Cl ages have been calculated using Excel spreadsheet of Schimmelpfening et al.
1000 (2009). N.M means no or incoherent measure. Maximum erosion rates have been calculated
1001 for the surface cobbles collected on T3 tread, with an infinite time of exposure hence at the
1002 steady state equilibrium. About 20-30 pebbles with centimetre size have been generally
1003 collected for the amalgamated samples of the profiles. For the T2/T0 riser profile, the
1004 amalgams are made of a dozen of larger cobbles.

1005

1006 Table 2: Mean chemical composition of the samples collected for ^{36}Cl dating. Measurements
1007 of the major elements were undertaken at the SARM facility (Nancy, France).

1008

1009 Table 3: Equivalent dose (D_e), annual dose rate (D_a) and calculated OSL ages for each sample.
1010 The weighted mean ages published in Nazari et al. (2009) have been refined following the
1011 statistical analysis used by Fattahi et al (2010) to account for partial bleaching. Ages have
1012 been calculated for Quartz grains with size ranging between 90 and 150 microns.

1013

1014

1015

Figure 1

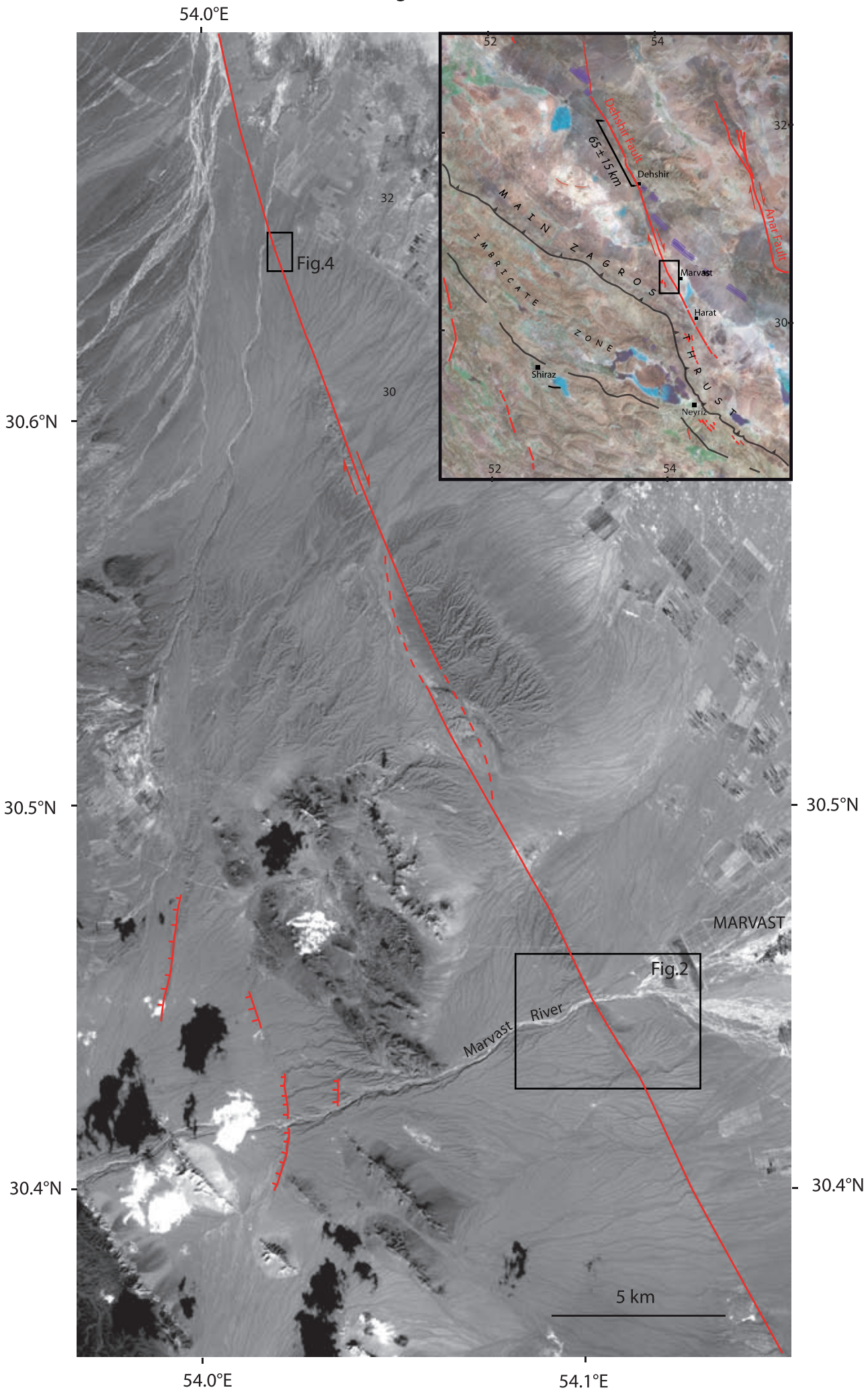


Figure 2

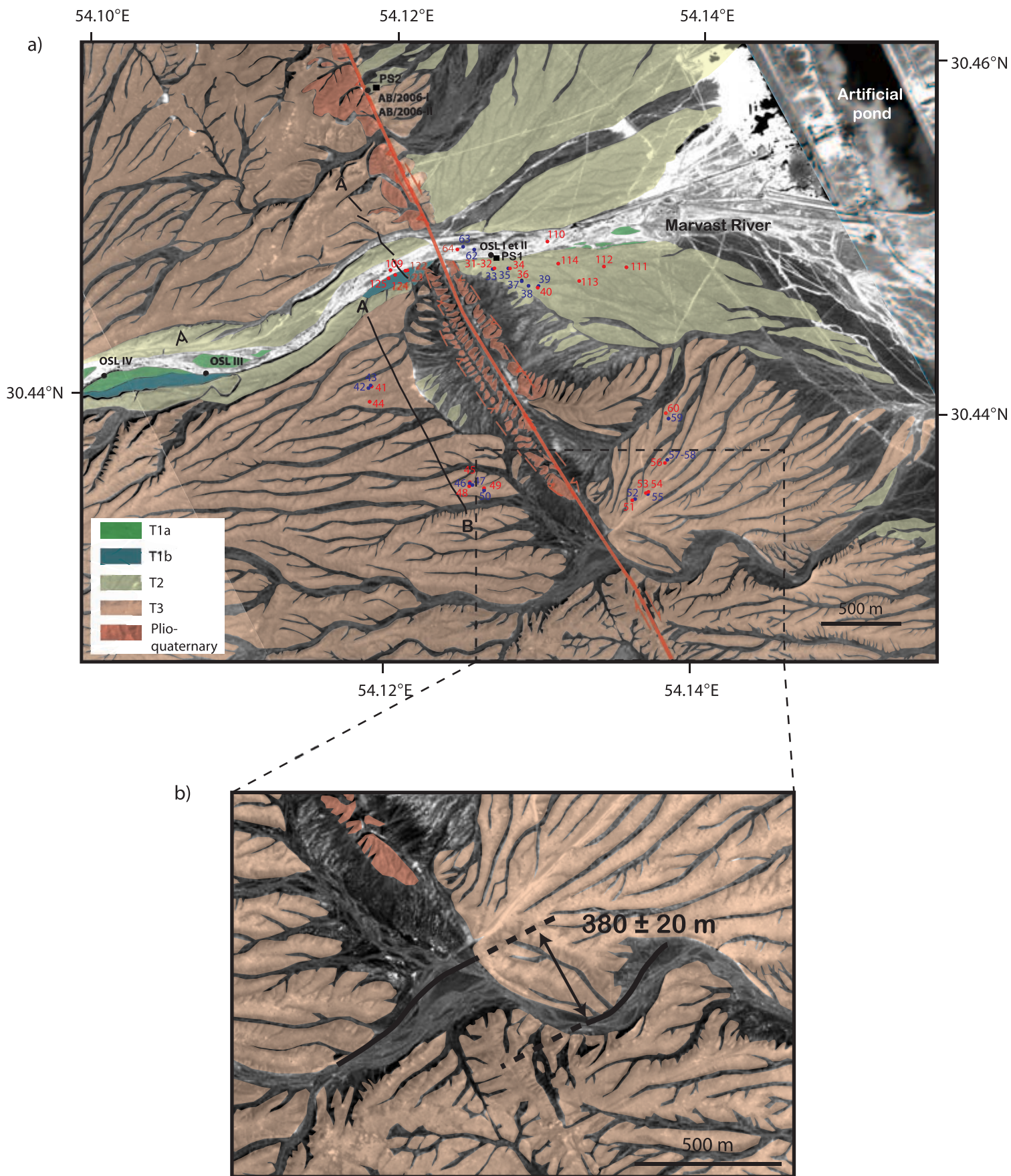
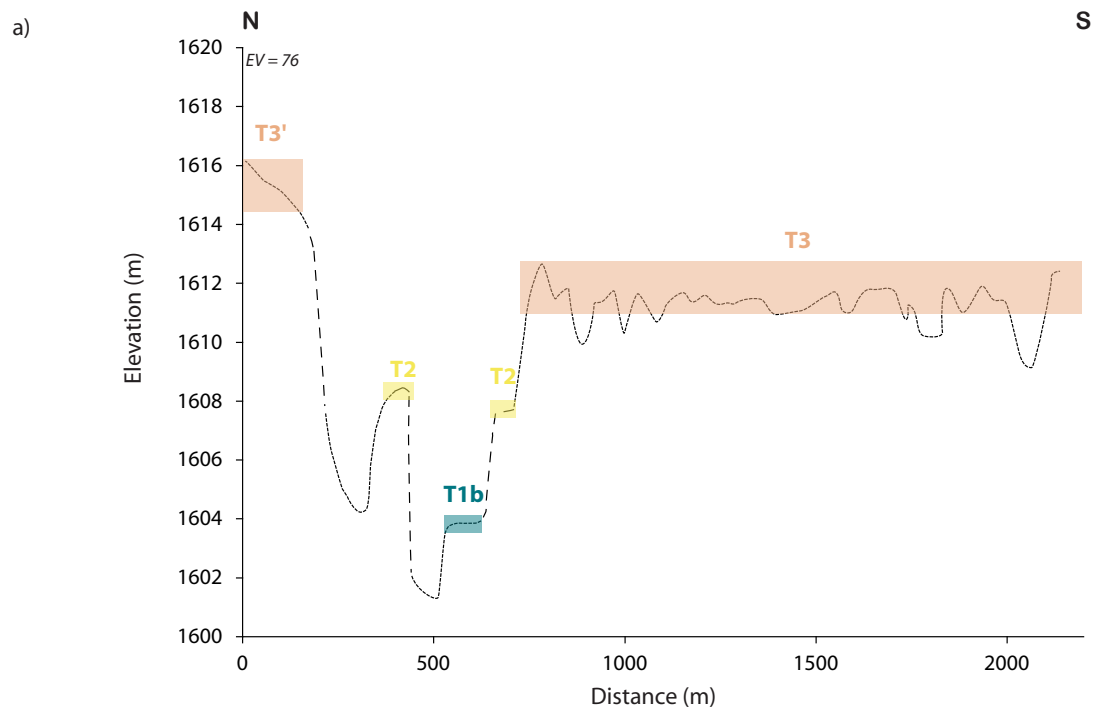


Figure 3



a)

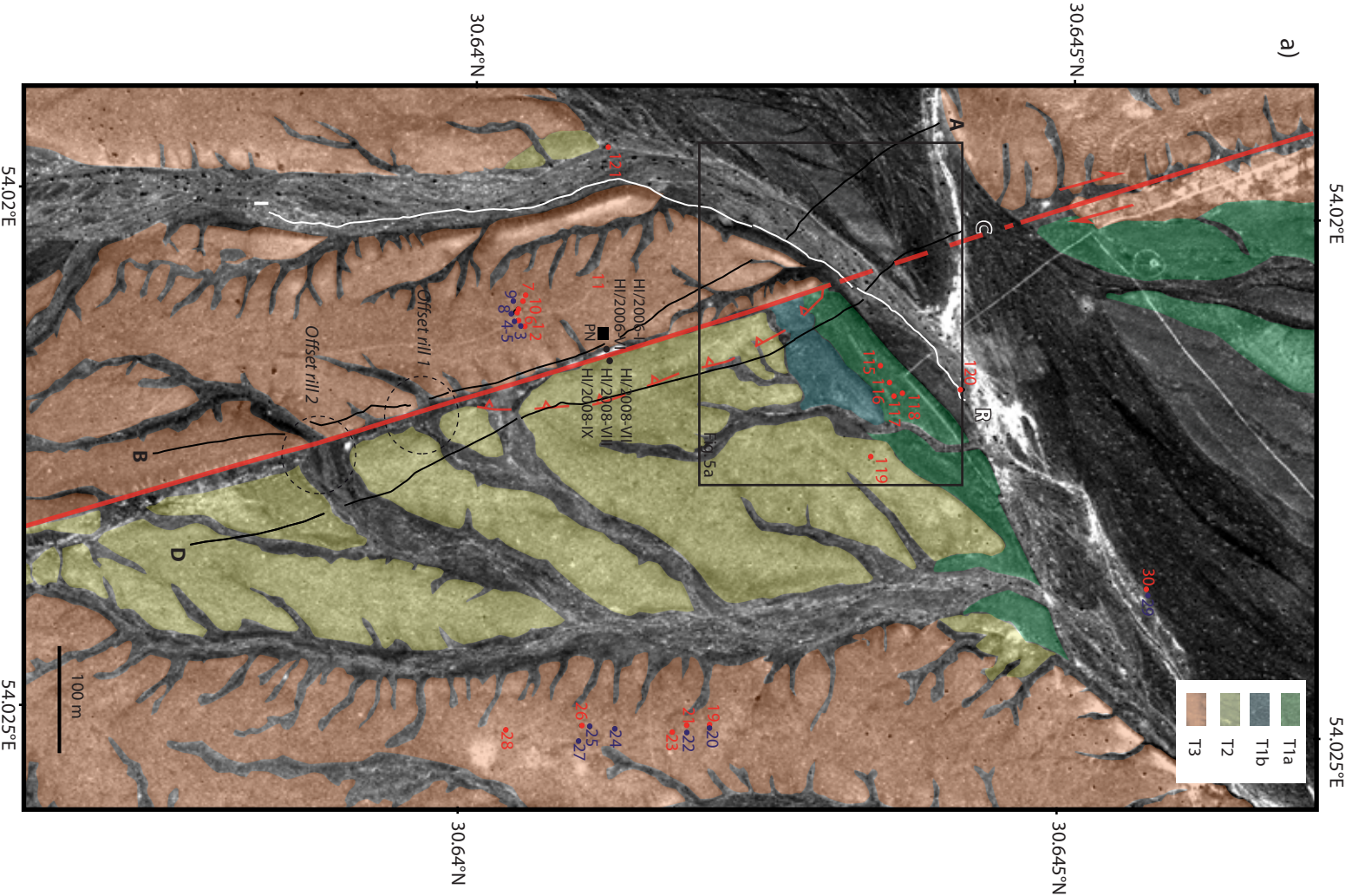


Figure 4

b)

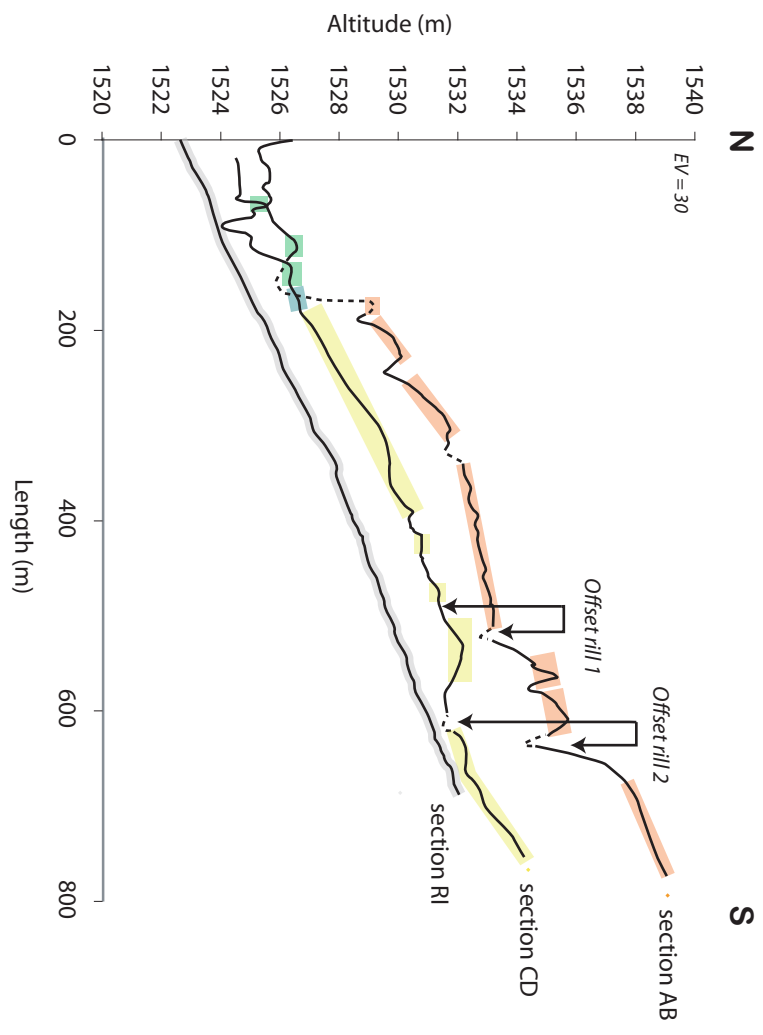
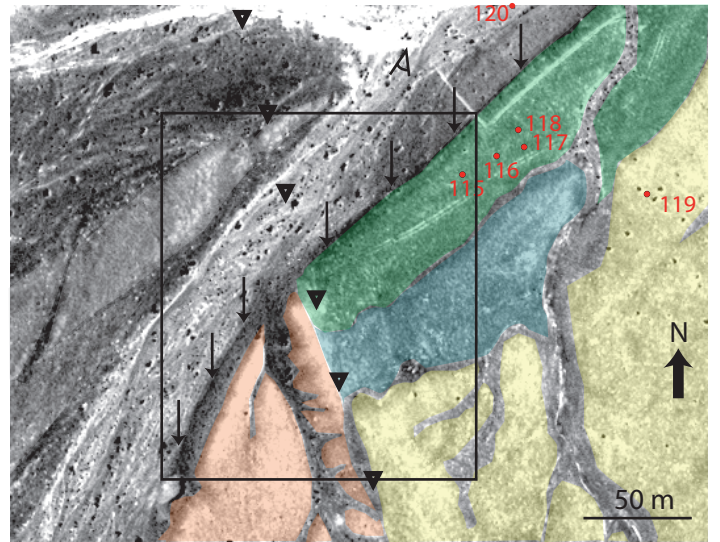
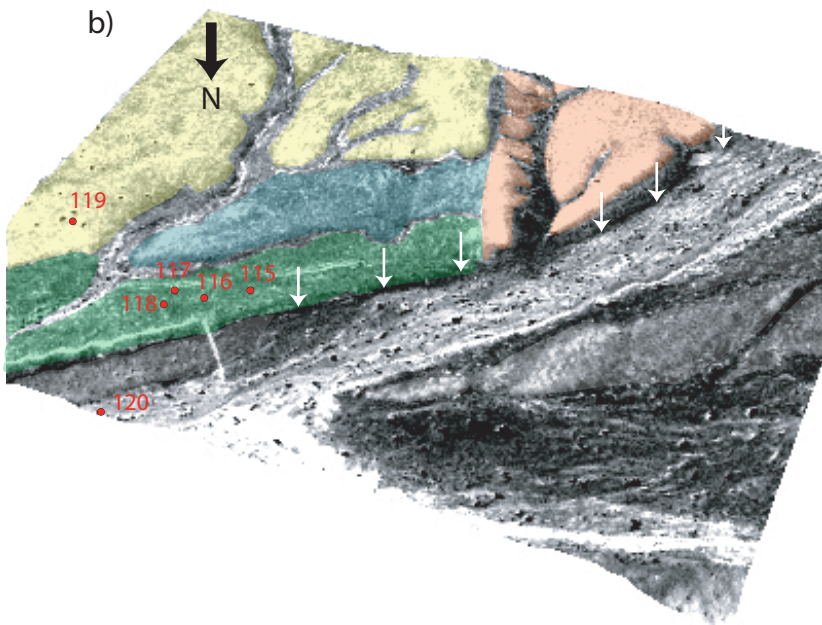


Figure 5

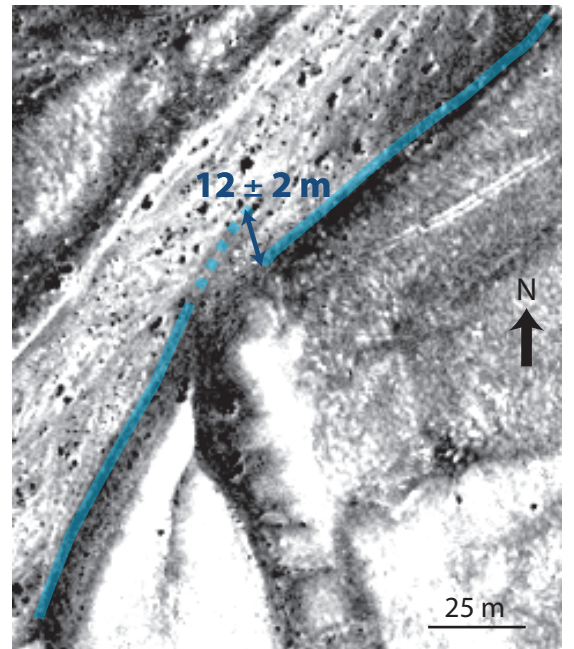
a)



b)



c)



d)

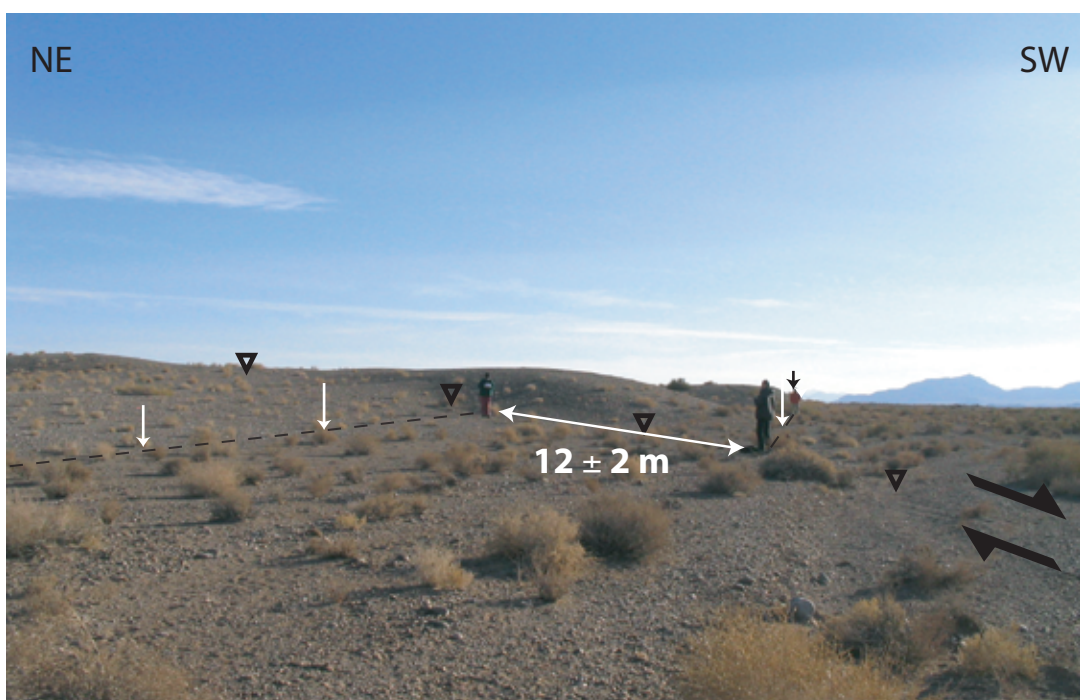
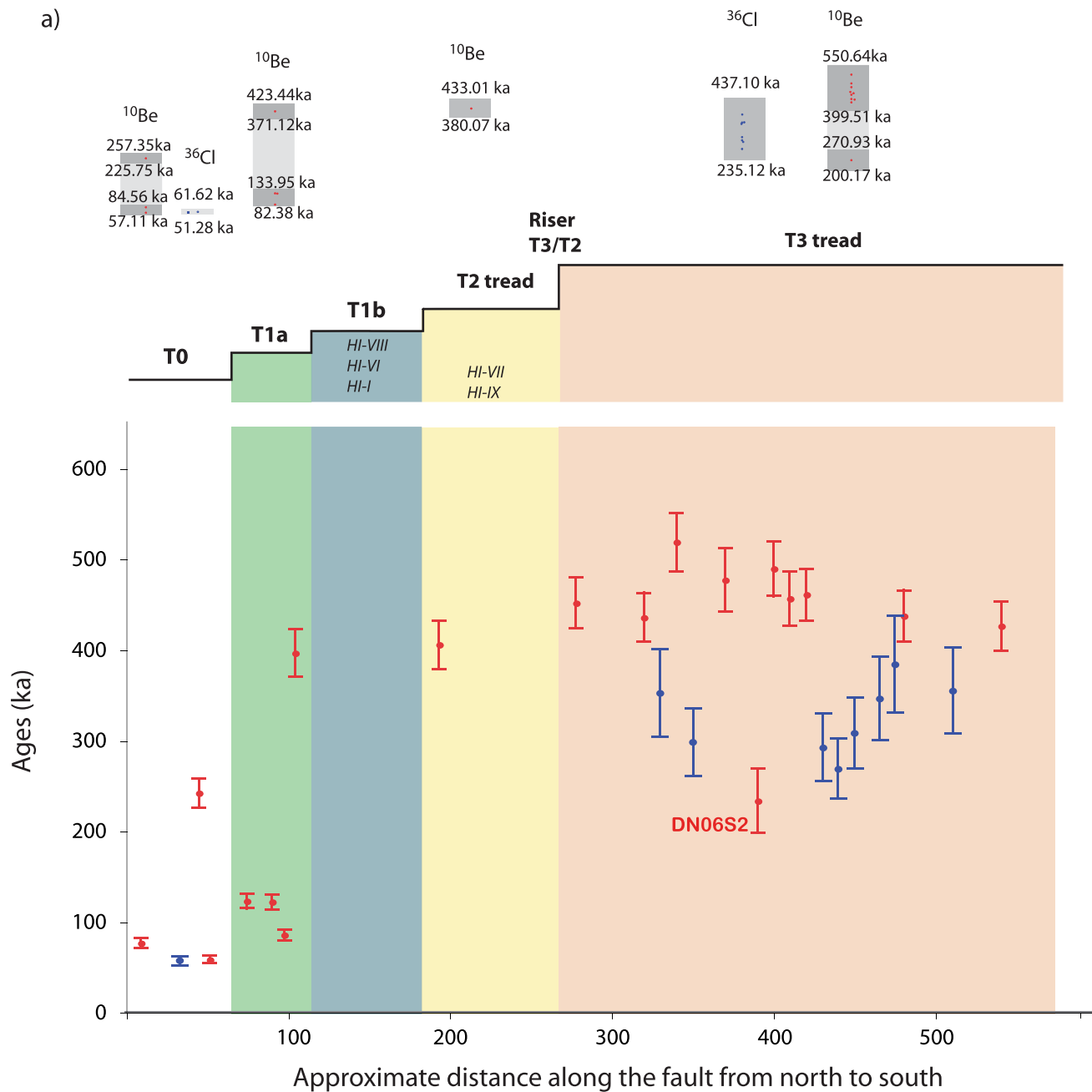


Figure 6

Dehshir North

a)



b) T3 tread

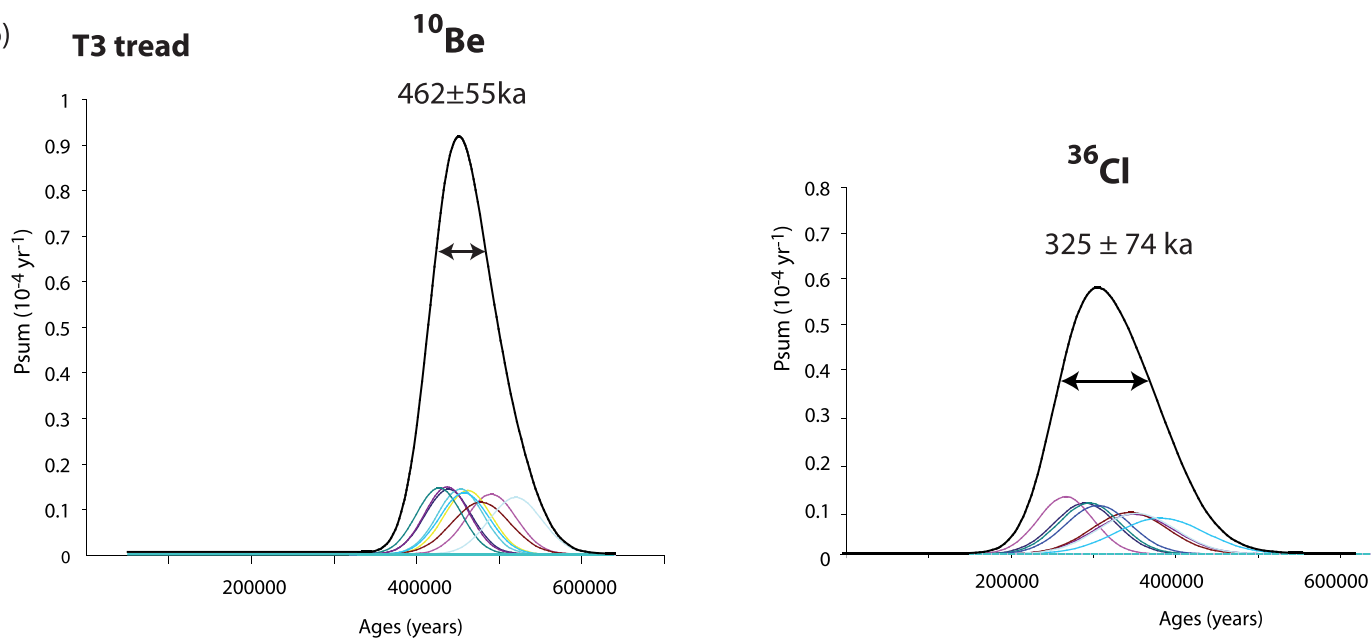
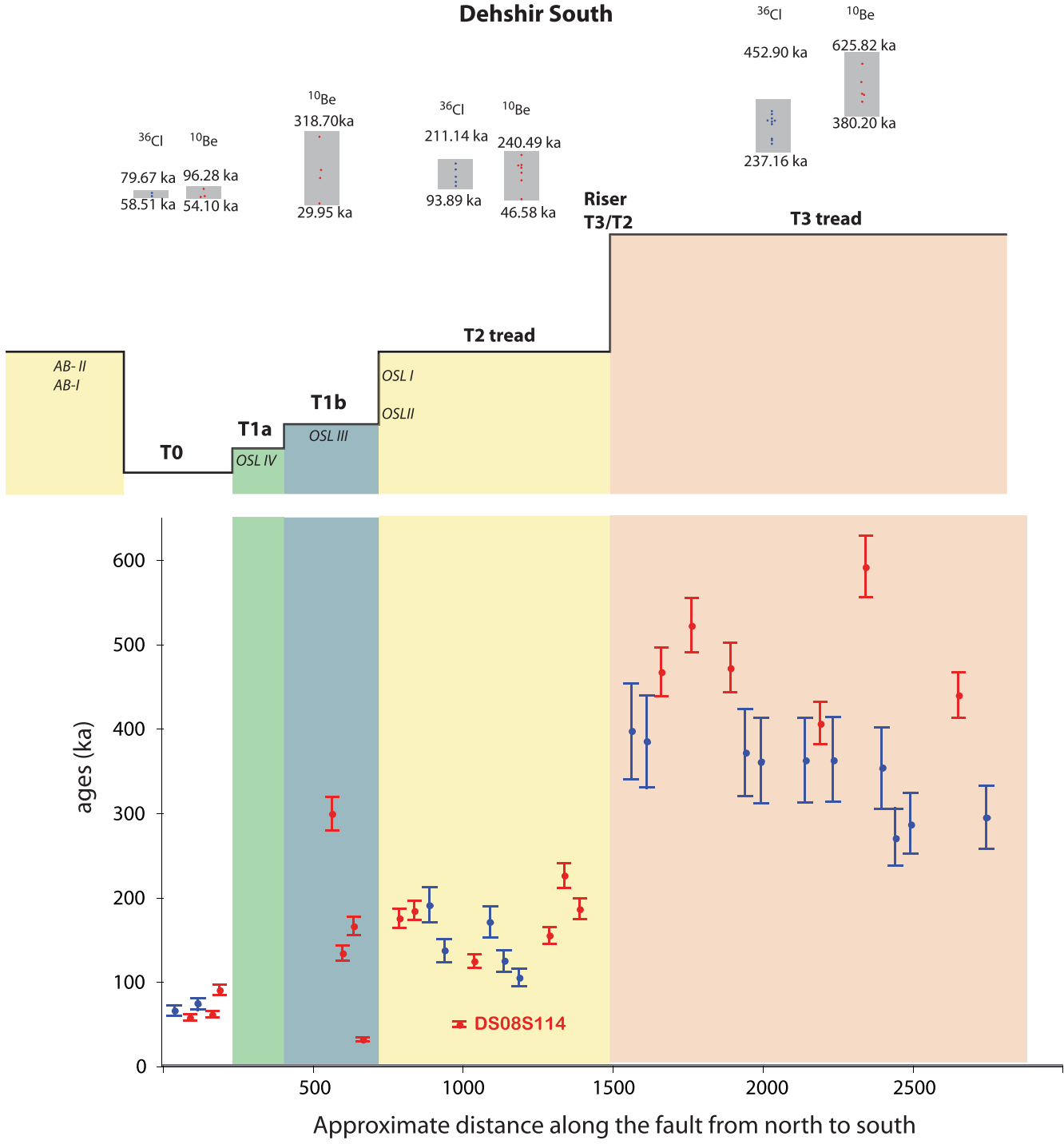


Figure 7
Dehshir South

a)



b) T3 tread

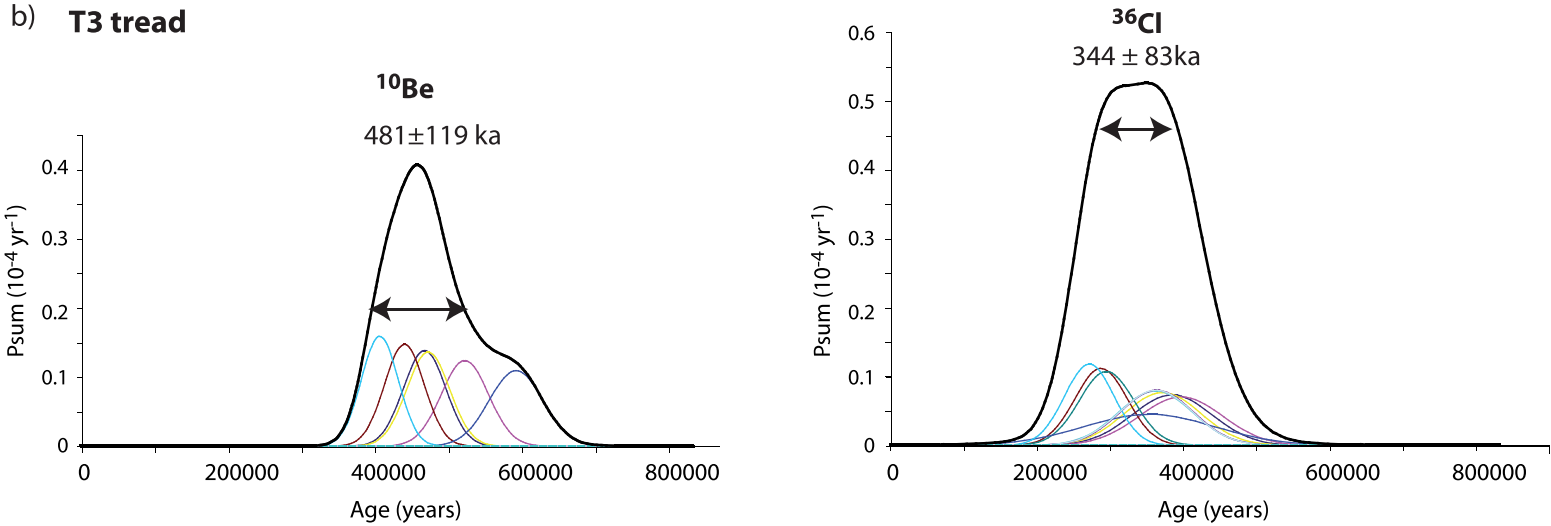


Figure 8

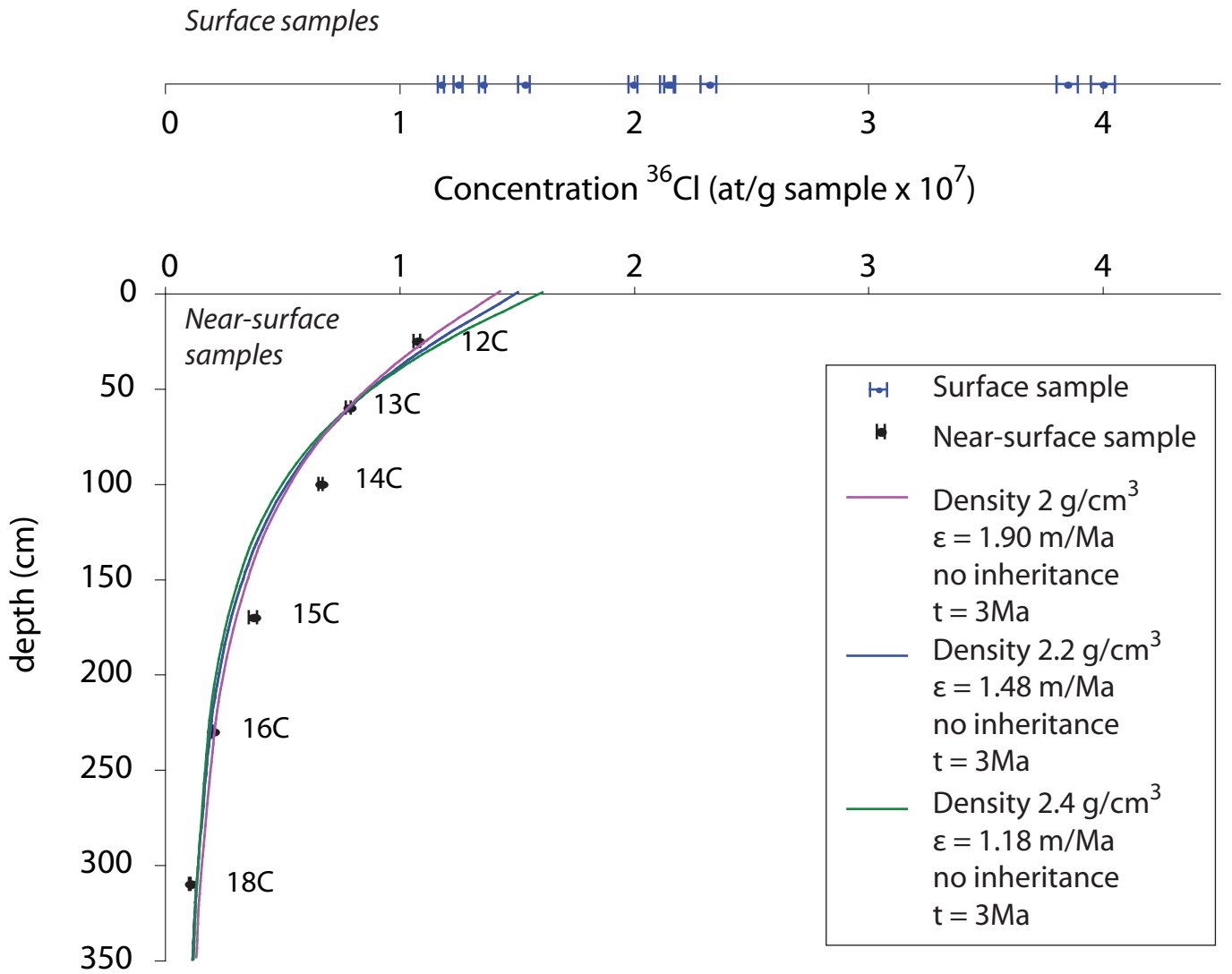


Figure 9

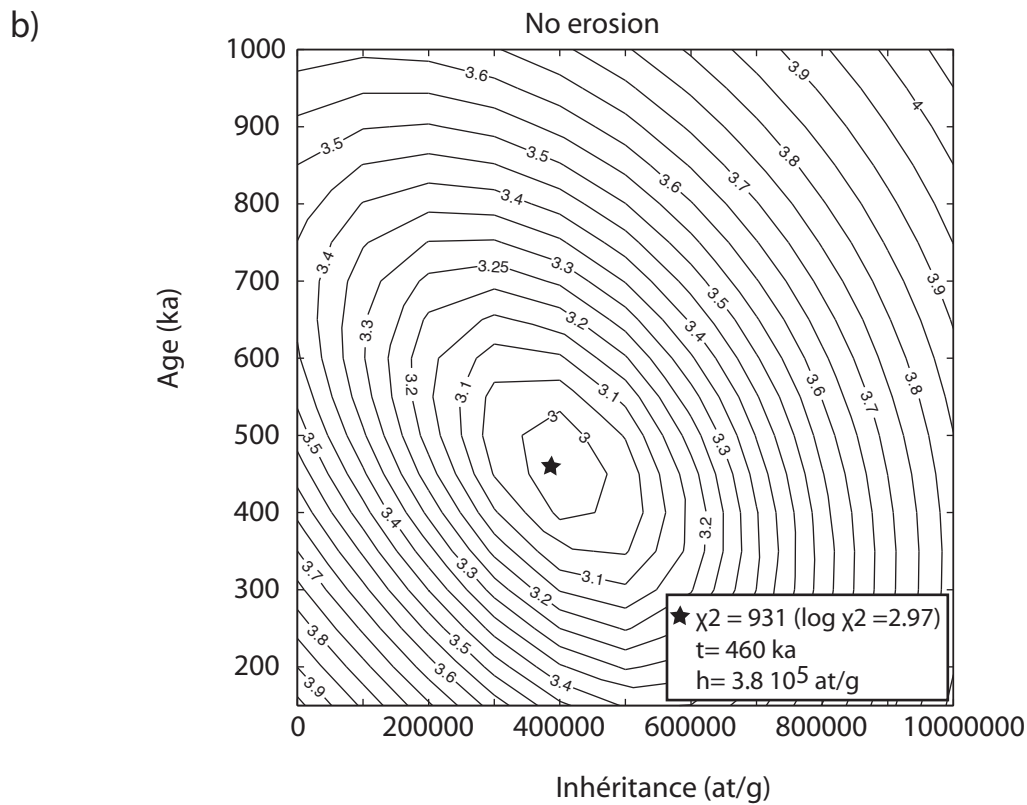
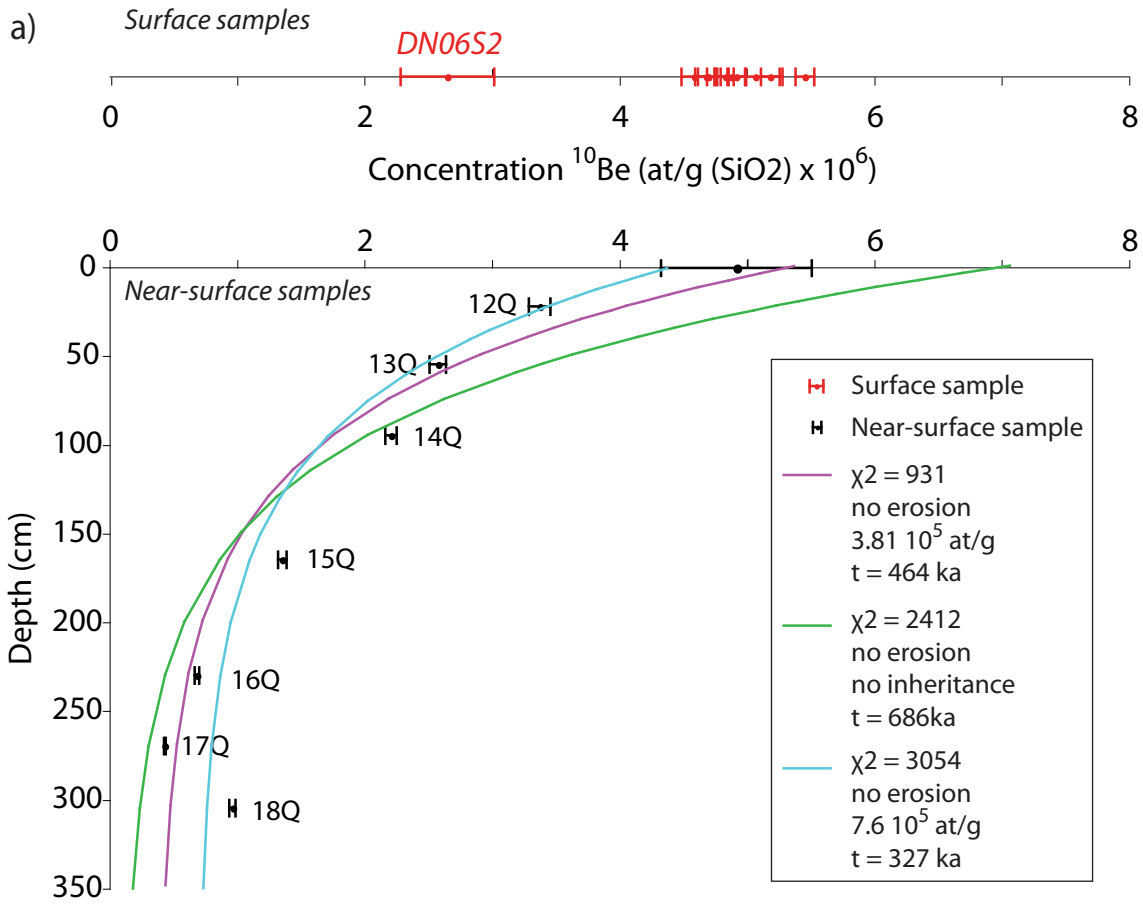


Figure 10

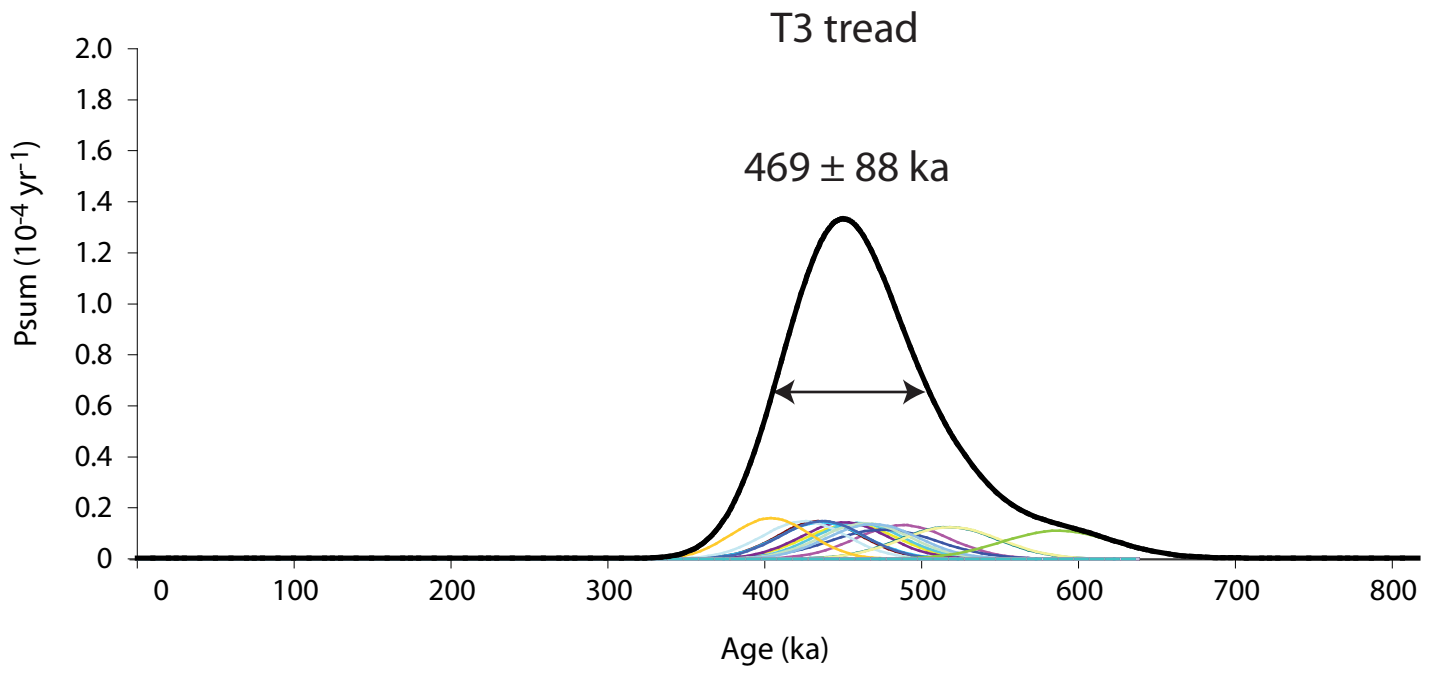


Figure 11

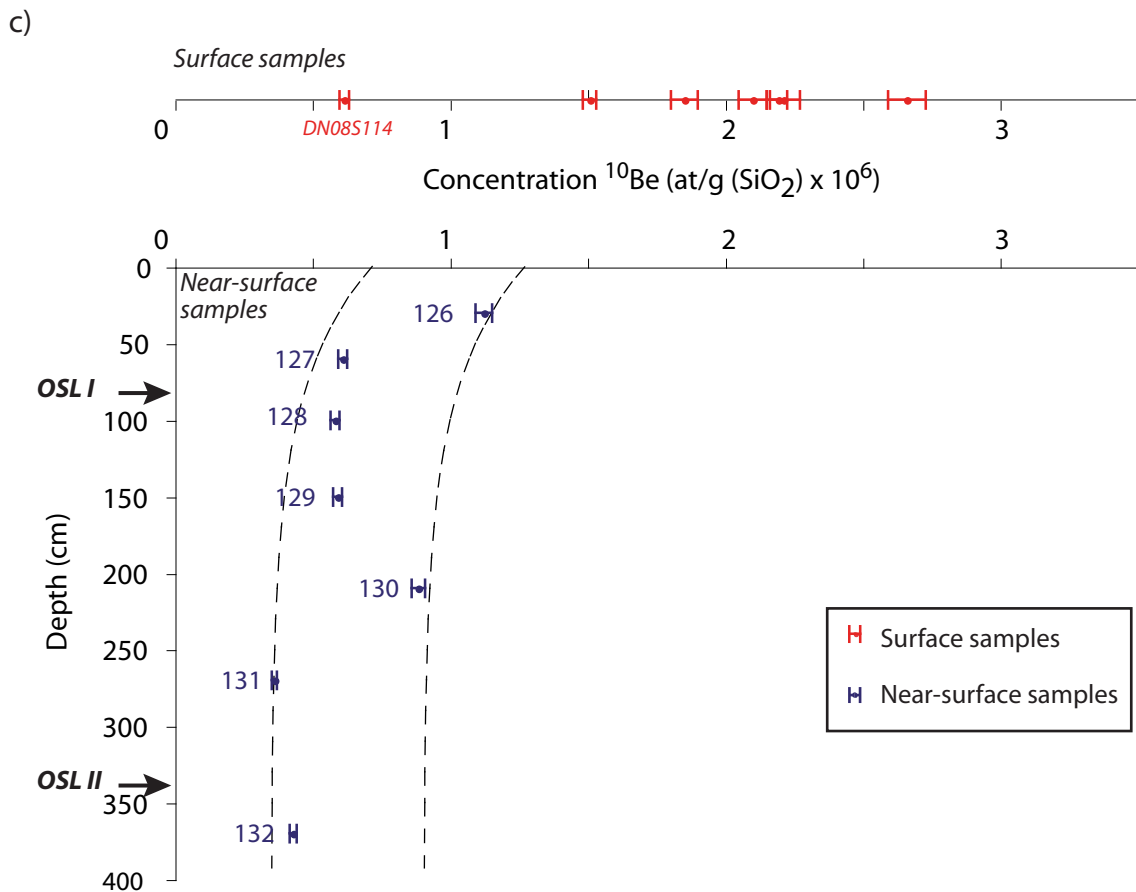
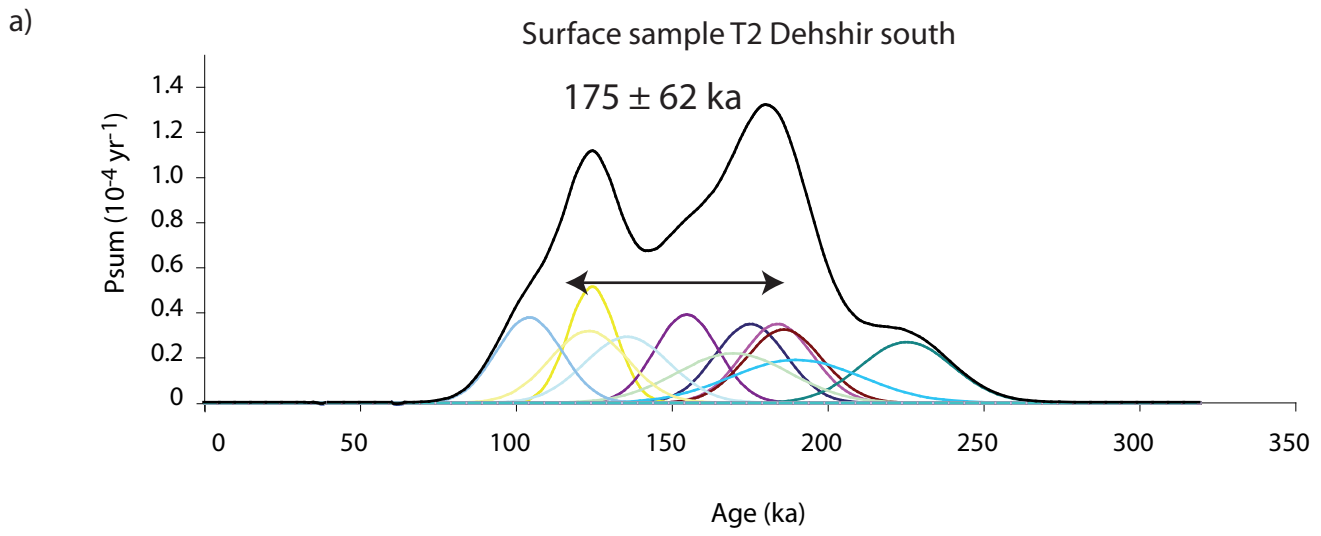


Figure 12

Profile PS2, Dehshir south T2

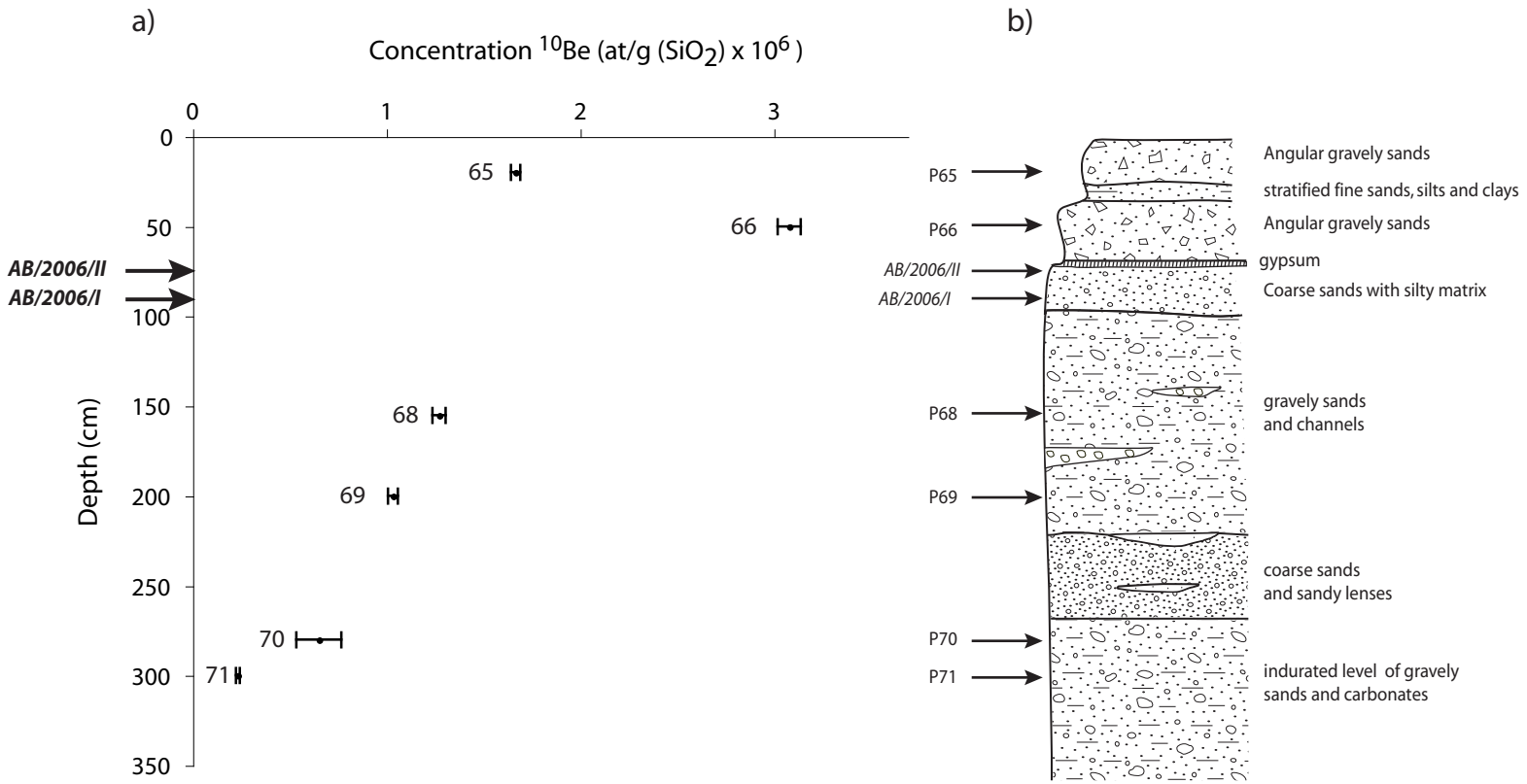


Figure 13

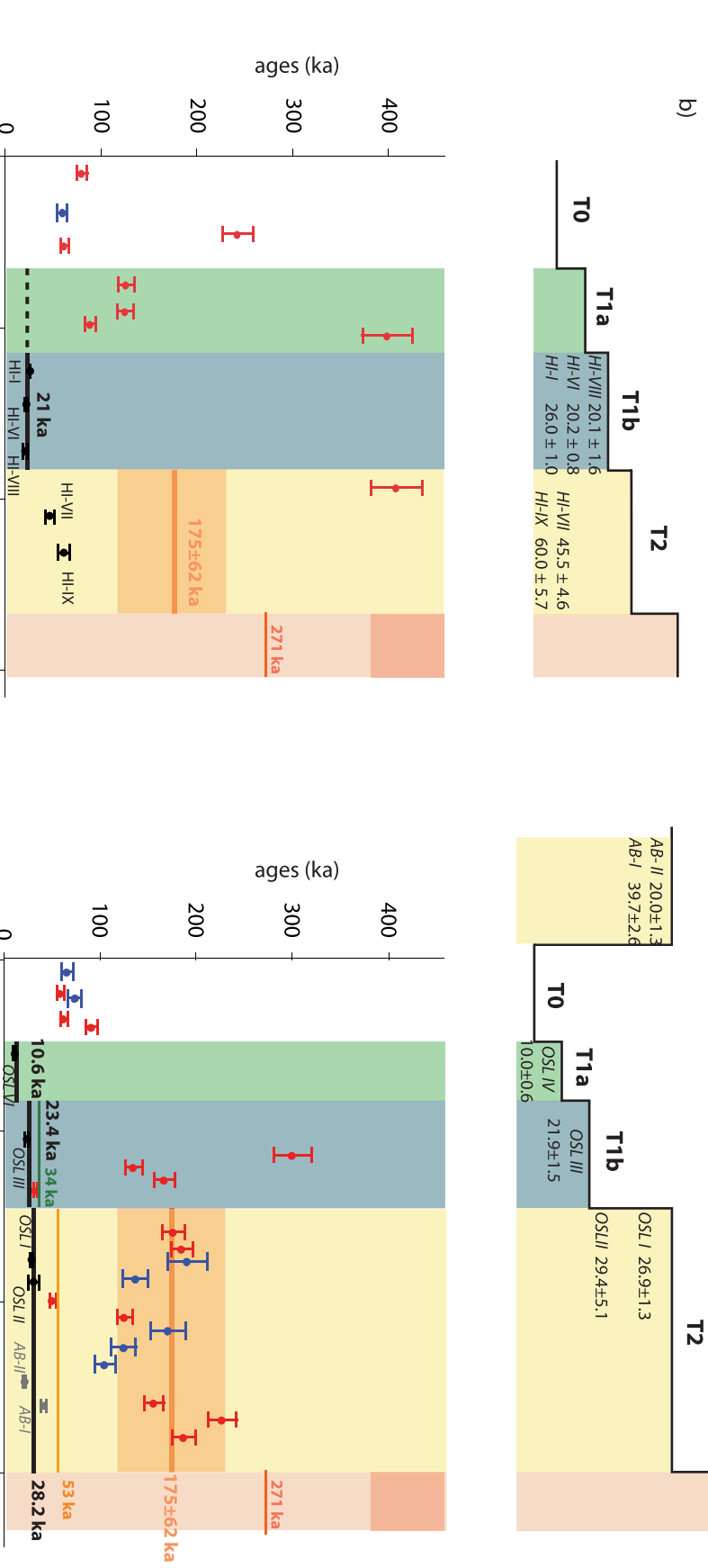
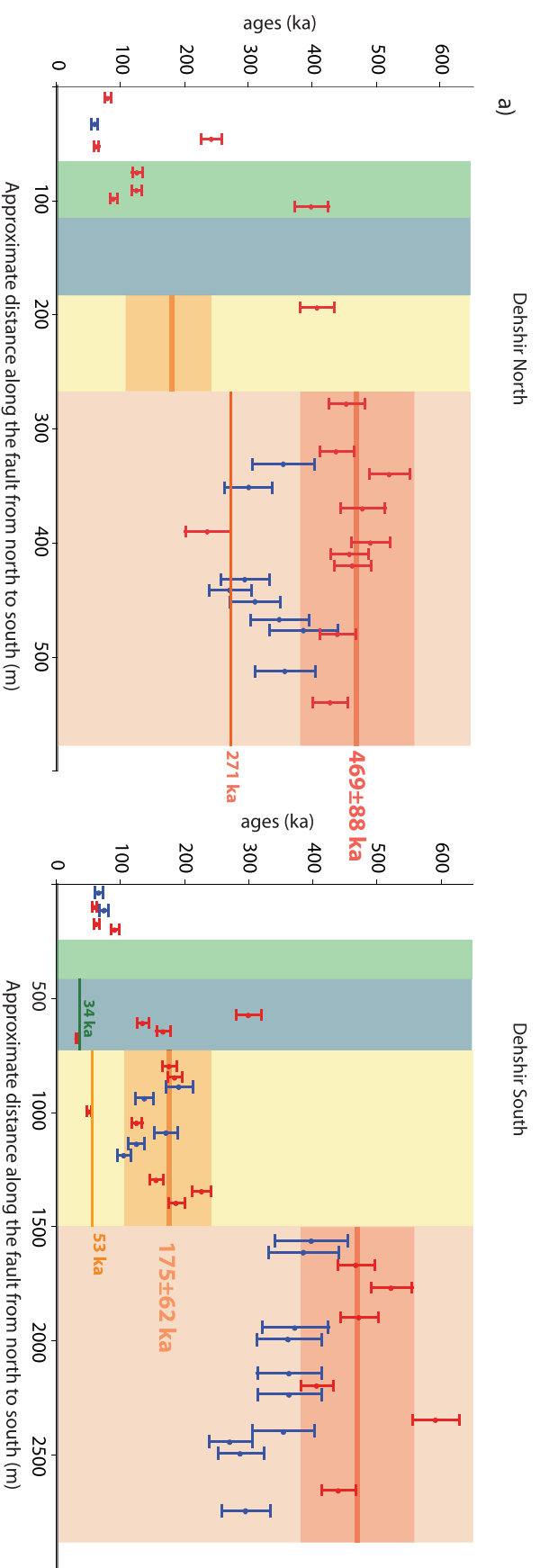


Figure 14

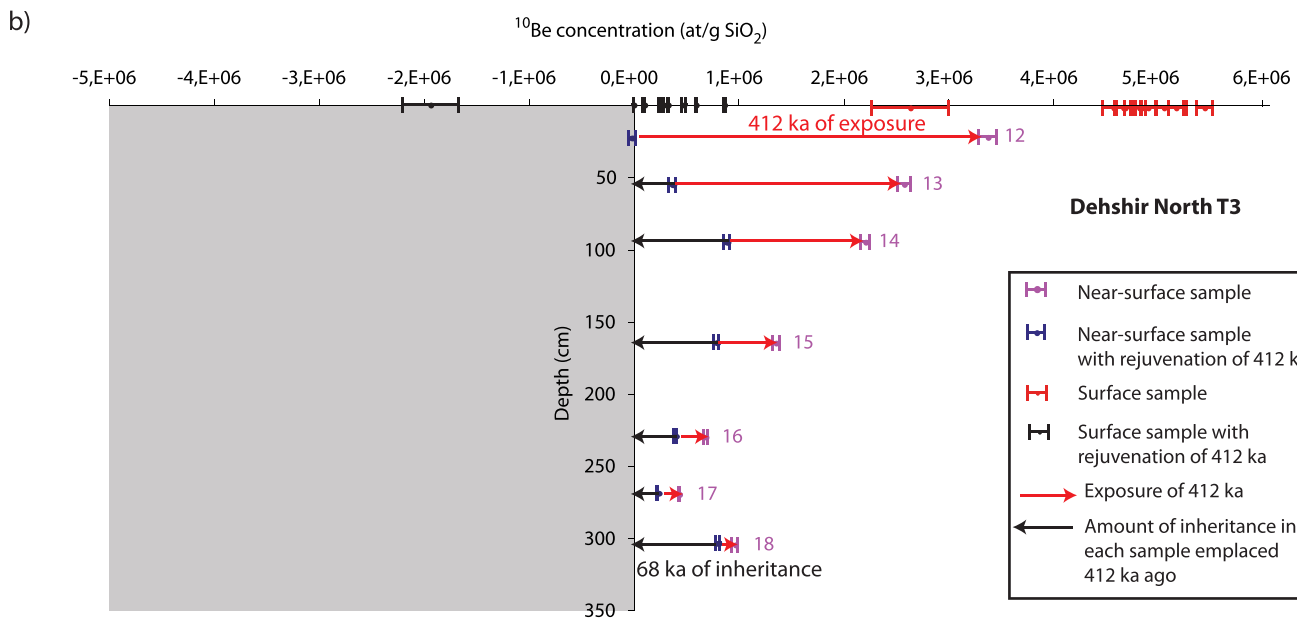
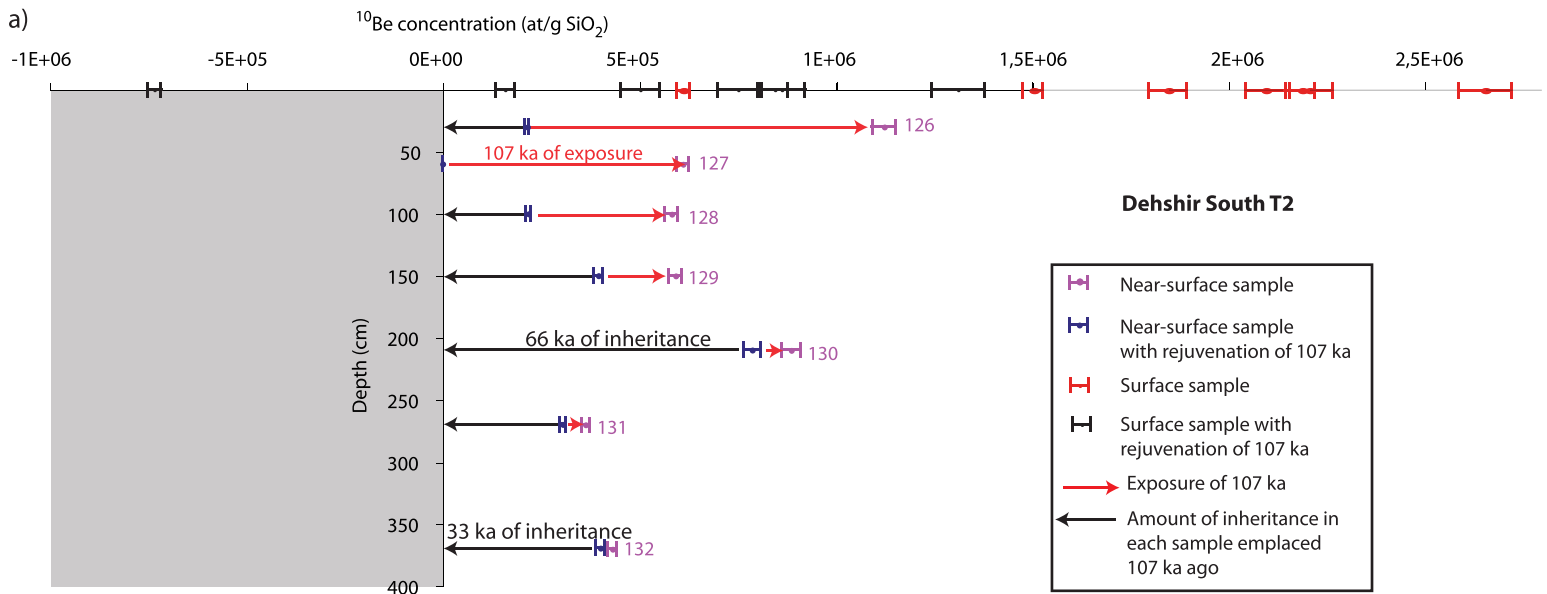
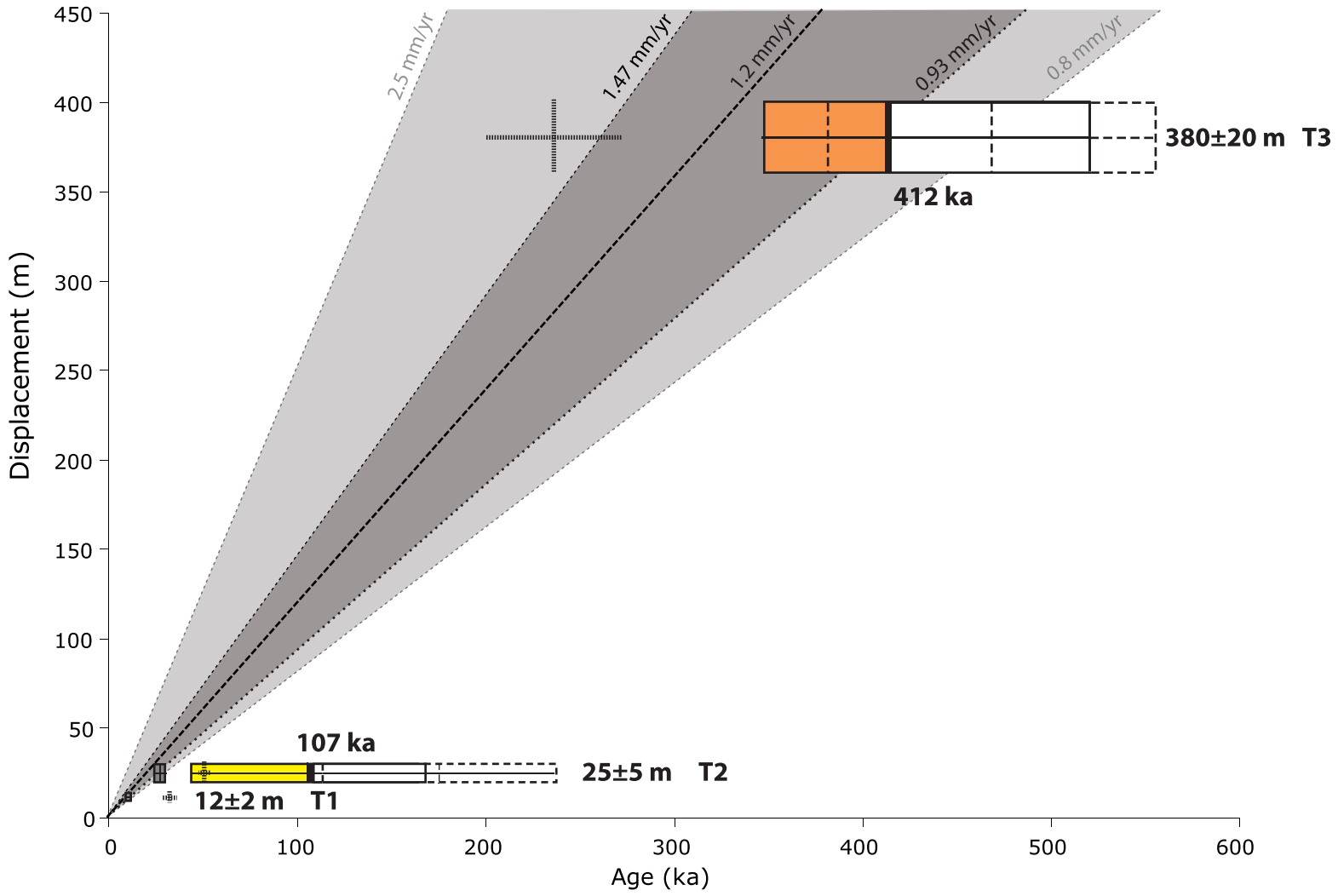


Figure 15



OSL Age

CRE weighted mean age

Maximum surface CRE age, with minimum inheritance removed from profile data



with and without modelled inheritance removed

CRE age of the youngest sample

Samples	Sample description	Density (g·cm ⁻³)	Thickness (cm)	Latitude (°N)	Longitude (°E)	Elevation (m)	¹⁰ Be			³⁶ Cl				
							Stone scaling factor	Measured ¹⁰ Be (10 ⁶ at.g ⁻¹ SiO ₂)	¹⁰ Be model age (ka) no erosion	¹⁰ Be maximum erosion rate (m·Ma ⁻¹)	Cl (ppm)	Measured ³⁶ Cl (10 ⁷ at.g ⁻¹ rock)	³⁶ Cl model age (ka) no erosion	³⁶ Cl maximum erosion rate (m·Ma ⁻¹)
Dahshir North														
T0														
DN06S30	cobble (15 cm) in the river bed	2.2	6	30.6457	54.0236	1539	2.64	9.23±0.22	79.42±5.14	8.98				
DN08S120	cobble (10 cm) in the river bed	2.2	8	30.6444	54.02172	1548	2.65	27.16±0.71	241.55±15.80	3.16				
DN08S121	cobble (15 cm) in the river bed	2.2	7	30.64111	54.01947	1547	2.65	7.18±0.19	61.15±4.03	14.30				
DN06S29	cobble (15 cm) in the river bed	2	7	30.64571	54.02366	1539					52	0.32±0.005	56.40±5.16	17.16
T1														
DN08S115	cobble (10 cm)	2.2	6	30.64343	54.02151	1550	2.66	43.06±1.17	397.28±26.16	1.79				
DN08S116	cobble (10 cm)	2.2	6	30.64351	54.02167	1549	2.65	10.30±0.28	88.19±5.81	9.62				
DN08S117	cobble (10 cm)	2.2	7	30.64355	54.0218	1550	2.66	14.42±0.39	124.44±8.19	6.60				
DN08S118	cobble (15 cm)	2.2	6	30.64362	54.02177	1549	2.65	14.55±0.39	125.69±8.26	6.53				
T2														
DN08A119	Amalgam (25 pluricentimetric clasts)	2.2	-	30.64337	54.02239	1550	2.66	43.97±1.11	406.54±26.47	1.74				
T3														
DN06S1	cobble (10 cm)	2.2	3	30.64068	54.01913	1550	2.72	N.M.	-	-				
DN06S2	2 fragments of the same gelyfracted cobble	2.2	3	30.64065	54.01907	1550	2.66	26.55±3.66	235.55±33.38	2.91				
DN06S6	cobble (10 cm)	2.2	5	30.640361	54.021083	1550	2.66	51.88±0.72	489.51±30.15	1.31				
DN06S7	cobble (15 cm)	2.2	4	30.64045	54.02092	1550	2.66	48.78±1.19	456.66±29.58	1.42				
DN06S10	cobble (10 cm)	2.2	5	30.6405	54.020917	1550	2.66	49.21±0.69	461.15±28.42	1.40				
DN06A11	Amalgam (20 pluricentimetric clasts)	2.2	-	30.6405	54.020917	1550	2.66	48.37±0.66	452.25±27.83	1.43				
DN06S19	cobble (10 cm)	2.2	4	30.64208	54.02502	1550	2.66	46.84±0.65	436.33±26.88	1.49				
DN06S21	cobble (10 cm)	2.2	4	30.64189	54.02503	1550	2.66	54.60±0.75	518.71±31.93	1.23				
DN06S23	cobble (10 cm)	2.2	7	30.64177	54.0251	1550	2.66	50.72±2.12	477.09±34.88	1.35				
DN06S26	cobble (10 cm)	2.2	8	30.64101	54.02506	1550	2.66	46.99±1.02	437.88±27.94	1.49				
DN06S28	cobble (20 cm)	2.2	9	30.64038	54.02512	1550	2.66	45.92±0.99	426.74±27.23	1.53				
DN06S3	cobble (10 cm)	2	8	30.640417	54.021222	1554					16	1.21±0.011	291.88±37.60	1.80
DN06S4	cobble (10 cm)	2	5	30.640333	54.021083	1556					18	1.18±0.014	268.43±33.33	2.10
DN06S5	2 fragments of the same gelyfracted cobble	2	4	30.640333	54.021083	1556					26	N.M.	-	-
DN06S8	cobble (15 cm)	2	3	30.640389	54.021055	1555					28	N.M.	-	-
DN06S9	cobble (10 cm)	2	5	30.640361	54.020972	1552					13	1.30±0.018	351.98±48.07	1.33
DN06S20	cobble (10 cm)	2	5	30.64208	54.02504	1550					24	1.36±0.013	345.97±45.90	1.48
DN06S22	cobble (10 cm)	2	3	30.64189	54.0251	1550					19	1.25±0.019	297.22±37.59	1.79
DN06S24	cobble (10 cm)	2	3	30.64129	54.02508	1549					18	1.31±0.014	307.95±39.30	1.68
DN06S25	cobble (10 cm)	2	3	30.64108	54.02507	1550					40	1.53±0.024	383.59±53.46	1.40
DN06S27	cobble (10 cm)	2	4	30.64099	54.02521	1550					38	1.41±0.02	354.70±47.24	1.57

Samples	Sample description	Density (g cm ⁻³)	Thickness (cm)	Latitude (°N)	Longitude (°E)	Elevation (m)	¹⁰ Be				³⁶ Cl				
							Stone scaling factor	Measured ¹⁰ Be (10 ⁶ at.g. ⁻² SiO ₂)	¹⁰ Be model age (ka) no erosion	¹⁰ Be maximum erosion rate (m.Ma ⁻¹)	Cl (ppm)	Measured ³⁶ Cl (10 ⁷ at.g. ⁻¹ rock)	³⁶ Cl model age (ka). no erosion	³⁶ Cl maximum erosion rate (m.Ma ⁻¹)	
Debshir South															
T0															
DS06S64	cobble (15 cm) in the river bed	2.2	7	30.44864	54.12418	1620	2.77	7.11±0.15	57.78±3.68	12.41	60	0.45±0.007	72.83±6.82	12.94	
DS08S109	cobble (15 cm) in the river bed	2.2	5	30.44742	54.11986	1626	2.79	7.63±0.21	61.83±4.08	14.13	10	1.44±0.013	271.00±33.83	1.92	
DS08S110	cobble (15 cm) in the river bed	2.2	6	30.44926	54.13	1613	2.76	10.97±0.29	90.34±5.94	9.37	8	1.41±0.011	362.38±49.94	1.22	
DS06S62	cobble (10 cm) in the river bed	2	4	30.44866	54.12527	1615					52	0.40±0.012	65.04±6.54	14.45	
DN06S63	cobble (10 cm) in the river bed	2	5	30.44881	54.12454	1615									
T1															
DS08S122	cobble (10 cm)	2.2	4	30.44743	54.12096	1626	2.79	34.77±0.93	298.60±19.60	2.48					
DS08S123	cobble (15 cm)	2.2	7	30.44741	54.12083	1626	2.79	19.96±0.52	165.94±10.87	4.80					
DS08S124	cobble (10 cm)	2.2	6	30.44716	54.12017	1627	2.79	3.99±0.11	32.07±2.12	28.42					
DS08S125	cobble (15 cm)	2.2	6	30.44695	54.11975	1627	2.79	16.28±0.44	134.22±8.83	6.07					
T2															
DS06S31	cobble (10 cm)	2.2	4	30.4476	54.12655	1622	2.78	N.M	-	-					
DS06S32	cobble (10 cm)	2.2	5	30.4476	54.12655	1622	2.78	21.01±0.52	175.57±11.39	3.96					
DS06S34	cobble (20 cm)	2.2	6	30.44765	54.12751	1619	2.77	21.95±0.32	184.19±11.38	3.77					
DS06S36	cobble (20 cm)	2.2	6	30.447	54.1284	1620	2.77	15.08±0.24	124.58±7.73	5.66					
DS06S40	cobble (10 cm)	2.2	5	30.44663	54.12945	1620	2.77	N.M	-	-					
DS08S111	cobble (10 cm)	2.2	6	30.44792	54.13517	1612	2.76	18.52±0.49	154.99±10.15	5.18					
DS08S112	cobble (10 cm)	2.2	7	30.44793	54.13371	1615	2.76	22.12±0.60	186.22±12.26	4.22					
DS08S113	cobble (10 cm)	2.2	7	30.44708	54.13213	1618	2.77	26.61±0.68	225.76±14.73	3.41					
DS08S114	cobble (10 cm)	2.2	6	30.44803	54.13074	1623	2.78	6.16±0.17	49.87±3.29	17.80	24	0.97±0.009	190.26±20.80	3.38	
DS06S33	cobble (15 cm)	2	7	30.44759	54.1265	1620					52	0.76±0.009	135.85±13.57	6.01	
DS06S35	cobble (20 cm)	2	4	30.44764	54.12754	1621					23	0.87±0.009	170.02±18.11	3.92	
DS06S37	cobble (10 cm)	2	5	30.44695	54.1284	1620					43	0.67±0.008	123.50±12.49	6.50	
DS06S38	cobble (10 cm)	2	4	30.44669	54.12885	1615					11	0.57±0.009	104.41±10.51	6.89	
DS06S39	cobble (10 cm)	2	4	30.44663	54.12946	1620									
T3															
DS06S41	2 fragments of the same gelyfracted cobble						2.2								
DS06S44	cobble (15 cm)	2.2	8	30.4408	54.11883	1632	2.80	52.28±0.75	465.68±28.72	1.39					
DS06S45	cobble (15 cm)	2.2	5	30.43993	54.11873	1636	2.80	57.81±0.81	520.28±32.06	1.22					
DS06S48	cobble (15 cm)	2.2	8	30.43552	54.12536	1632	2.80	52.76±0.84	470.58±29.21	1.37					
DS06S49	cobble (20 cm)	2.2	9	30.43552	54.12533	1630	2.79	N.M	-	-					
DS06S51	2 fragments of the same gelyfracted cobble						2.2								
DS06S53	cobble (10 cm)	2.2	6	30.43518	54.1263	1630	2.79	N.M	-	-					
DS06S54	cobble (10 cm)	2.2	5	30.43475	54.13594	1620	2.77	N.M	-	-					
DS06S54	cobble (15 cm)	2.2	5	30.43517	54.13687	1623	2.78	49.22±0.66	438.32±26.95	1.48					
DS06S54	cobble (15 cm)	2.2	6	30.43521	54.13694	1618	2.77	N.M	-	-					
DS06S56	cobble (10 cm)	2.2	8	30.4369	54.138	1620	2.77	63.71±0.90	589.48±36.34	1.06					
DS06S60	cobble (15 cm)	2.2	7	30.43971	54.13797	1620	2.77	45.77±0.65	405.18±24.98	1.62					
DS06S42	1 fragment of a gelyfracted cobble (15 cm)						2.2								
DS06S43	cobble (15 cm)	2	4	30.4407	54.11873	1630					17	1.51±0.022	384.20±54.50	1.19	
DS06S46	cobble (10 cm)	2	5	30.44082	54.11877	1632					17	1.55±0.015	396.25±56.62	1.13	
DS06S47	cobble (15 cm)	2	3	30.43548	54.12536	1630					14	1.54±0.014	371.29±52.05	1.21	
DS06S50	cobble (15 cm)	2	3	30.43538	54.12553	1630					14	1.46±0.034	361.52±50.52	1.40	
DS06S52	cobble (15 cm)	2	4	30.4351	54.12631	1631					18	1.45±0.016	363.29±49.85	1.03	
DS06S52	cobble (10 cm)	2	4	30.43482	54.13612	1625					16	1.24±0.014	287.11±35.74	1.84	
DS06S55	cobble (15 cm)	2	5	30.43515	54.13692	1626					17	1.27±0.020	294.57±37.25	1.79	
DS06S57	cobble (10 cm)	2	5	30.43708	54.13814	1627					10	1.44±0.013	352.98±48.02	1.29	
DS06S58	cobble (15 cm)	2	8	30.43708	54.13814	1627					10	1.19±0.023	271.00±33.83	1.92	
DS06S59	cobble (10 cm)	2	6	30.43941	54.13816	1625					8	1.41±0.011	362.38±49.94	1.22	

Samples	H ₂ O %	Al ₂ O ₃ %	CaO %	Fe ₂ O ₃ %	K ₂ O %	MgO %	MnO %	Na ₂ O %	P ₂ O ₅ %	SiO ₂ %	TiO ₂ %	Th %	U %
DN06S3	0.30	0.04	54.38	0.15	0	0.59	0.01	0	0.02	0.11	0.00	0.020	0.763
DN06S4	0.35	0.15	53.85	0.08	0	0.90	0.02	0	0.02	0.21	0.01	0.113	2.740
DN06S5	0.29	0.09	54.39	0.10	0	0.68	0.01	0	0.02	0.11	0.00	0.064	1.295
DN06S8	0.22	0.07	54.92	0.08	0	0.57	0.01	0	0.02	0.00	0.01	0.058	0.382
DNS06S9	0.29	0.09	54.39	0.10	0	0.68	0.01	0	0.02	0.11	0.00	0.064	1.295
DN06P12C	0.41	0.40	52.75	0.33	0.09	0.92	0.02	0	0	1.99	0.03	0.309	1.164
DN06P13	0.41	0.40	52.75	0.33	0.09	0.92	0.02	0	0	1.99	0.03	0.309	1.164
DN06P14C	0.41	0.40	52.75	0.33	0.09	0.92	0.02	0	0	1.99	0.03	0.309	1.164
DN06P15C	0.41	0.40	52.75	0.33	0.09	0.92	0.02	0	0	1.99	0.03	0.309	1.164
DN06P16C	0.41	0.40	52.75	0.33	0.09	0.92	0.02	0	0	1.99	0.03	0.309	1.164
DN06P18C	0.41	0.40	52.75	0.33	0.09	0.92	0.02	0	0	1.99	0.03	0.309	1.164
DNO6S20	0.31	0.08	53.74	0.15	0	1.20	0.03	0	0	0.12	0.00	0.048	0.861
DN06S22	0.26	0.02	54.28	0.04	0	1.10	0.00	0	0	0.00	0.00	0.000	1.330
DNO6S24	0.31	0.08	53.74	0.15	0	1.20	0.03	0	0	0.12	0.00	0.048	0.861
DN06S25	0.36	0.14	53.20	0.26	0	1.31	0.05	0	0	0.24	0.01	0.095	0.392
DNO6S27	0.31	0.08	53.74	0.15	0	1.20	0.03	0	0	0.12	0.00	0.048	0.861
DNO6S29	0.31	0.08	53.74	0.15	0.00	1.20	0.03	0	0.00	0.12	0.00	0.048	0.861
DS06S33	0.245	0.022	54.39	0.06	0	0.652	0.0035	0	0.008	0	0	0.025	1.433
DS06S35	0.245	0.022	54.39	0.06	0	0.652	0.0035	0	0.008	0	0	0.025	1.433
DS06S37	0.245	0.022	54.39	0.06	0	0.652	0.0035	0	0.008	0	0	0.025	1.433
DS06S38	0.27	0.02	54.08	0.05	0	0.87	0.01	0	0.02	0.00	0.00	0.028	0.370
DS06S39	0.22	0.02	54.71	0.08	0	0.44	0.00	0	0.00	0.00	0.00	0.021	2.495
DS06S42	0.27	0.05	54.89	0	0	0.55	0	0	0	0	0.00	0.096	3.010
DSO6S43	0.27	0.05	54.89	0	0	0.55	0	0	0	0	0.00	0.096	3.010
DS06S46	0.27	0.05	54.89	0	0	0.55	0	0	0	0	0.00	0.096	3.010
DSO6S47	0.27	0.05	54.89	0	0	0.55	0	0	0	0	0.00	0.096	3.010
DS06S50	0.27	0.05	54.89	0	0	0.55	0	0	0	0	0.00	0.096	3.010
DNO6S52	0.28	0	54.60	0.12	0	0.38	0	0	0	0	0.00	0.020	2.995
DSO6S55	0.28	0	54.60	0.12	0	0.38	0	0	0	0	0.00	0.020	2.995
DS06S57	0.28	0	54.60	0.12	0	0.38	0	0	0	0	0.00	0.020	2.995
DSO6S58	0.28	0	54.60	0.12	0	0.38	0	0	0	0	0.00	0.020	2.995
DSO6S59	0.28	0	54.60	0.12	0	0.38	0	0	0	0	0.00	0.020	2.995
DS06S62	0.22	0.04	54.16	0.16	0.00	0.90	0.03	0.00	0.00	0.00	0.00	0.045	0.675
DS06S63	0.22	0.04	54.16	0.16	0.00	0.90	0.03	0.00	0.00	0.00	0.00	0.045	0.675

Sample	Latitude (°N)	Longitude (°E)	Depth (m)	Water (%)	K (%)	U (%)	Th (%)	Equivalent Dose CAM (Gy)	Equivalent Dose FMM* (Gy)	Annual dose rate (Gy.ka ⁻¹)	Age (ka)
Site Dehshir North											
Trench (alluviums coeval with T1 aggradation)											
HI/2006-VI	30.64121	54.02127	1.5	1.3	1.27±0.01	2.04±0.05	6.0±0.1	48.8±0.3		2.43±0.09	20.2±0.8 ^e
HI/2008-VIII	30.64123	54.02148	0.95	0.9	0.66±0.01	1.13±0.05	4.6±0.1	45.3±7.1	29.3±2.0	1.45±0.03	20.1±1.6 ^f
HI/2006-I	30.64118	54.02131	1.2	0.9	1.22±0.01	1.79±0.05	6.0±0.1	60.2±0.28		2.29±0.09	26.0±1.0 ^e
Trench (alluviums coeval with T2 aggradation)											
HI/2008-VII	30.64123	54.02145	1.6	1.1	0.61±0.01	1.1±0.05	4.3±0.1	62.0±6.0		1.36±0.03	45.5±4.6 ^e
HI/2008-IX	30.64123	54.02150	2.8	1.2	0.66±0.01	1.12±0.05	4.5±0.1	83.0±7.3		1.40±0.03	60.0±5.7 ^e
Site Dehshir South											
Riser T2/T0											
OSL I	30.44823	54.12632	0.8	1.1±0.2	0.78±0.01	1.52±0.05	4.8±0.1	46.5±1.4		1.73±0.04	26.9±1.3 ^e
OSL II	30.84823	54.12658	3.4	1.05±0.2	0.85±0.01	1.05±0.05	4.2±0.1	45.6±7.7		1.55±0.04	29.4±5.1 ^e
Riser T1b/T0											
OSL III	30.44132	54.10805	2.64	0.35±0.2	0.67±0.01	0.95±0.05	3.4±0.1	28.9±1.7		1.32±0.04	21.9±1.5 ^e
Riser T1a/T0											
OSL IV	30.44116	54.10173	0.8	0.2±0.2	0.71±0.01	1.15±0.05	5.0±0.1	23.4±2.6	15.7±0.8	1.57±0.04	10.0±0.6 ^f
Pit in the surface T2											
AB/2006-I	30.45719	54.11822	0.9	1.1±0.2	0.86±0.01	1.78±0.05	4.2±0.1	73.3±3.7	72.9±3.8	1.83±0.05	39.7±2.6 ^f
AB/2006-II	30.45719	54.11831	0.7	1.1±0.2	1.1±0.01	1.64±0.05	5.9±0.1	57.4±7.6	43.2±2.3	2.16±0.05	20.0±1.3 ^f

* Finite Mixture Modelling (Roberts et al 2000) of replicate De values only undertaken where De distributions were multimodal, skewed and/or scattered (see text for details).

^e Age based on De determined using Central age Model (CAM; Galbraith et al. 1999).

^f Age based on De determined using Finite mixture Modeling (FMM; Roberts et al 2000).